

Weierstraß-Institut für Angewandte Analysis und Stochastik

im Forschungsverbund Berlin e.V.

Preprint

ISSN 0946 – 8633

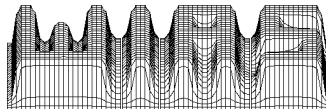
Numerical algorithms to calculate periodic solutions of the Sivashinsky equation

V. Karlin¹, V. Maz'ya², G. Schmidt³

submitted: 4th October 2002

- ¹ Centre for Research in Fire and Explosions,
University of Central Lancashire,
Preston PR1 2HE, UK,
E-Mail: VKarlin@uclan.ac.uk
- ² Department of Mathematics, Linköping University,
Linköping, S-581 83, Sweden,
E-Mail: vlmaz@math.liu.se
- ³ Weierstrass Institute for Applied Analysis and Stochastics,
Mohrenstrasse 39, D-10117 Berlin, Germany,
E-Mail: schmidt@wias-berlin.de

No. 771
Berlin 2002



1991 *Mathematics Subject Classification.* 65M70, 76E17, 65G50.

Key words and phrases. saturated asymptotic approximations, Sivashinsky equation, flame fronts, stability, round-off errors.

Edited by
Weierstraß-Institut für Angewandte Analysis und Stochastik (WIAS)
Mohrenstraße 39
D — 10117 Berlin
Germany

Fax: + 49 30 2044975
E-Mail: preprint@wias-berlin.de
World Wide Web: <http://www.wias-berlin.de/>

Abstract

The primary aim of this work is the accurate calculation of periodic solutions to the Sivashinsky equation, which models dynamics of the long wave flame instability. A highly accurate computational algorithm has been developed in both one and two spatial dimensions and its crucial implementation details has been presented. The algorithm is based on the concept of “approximate approximations” which also can be referred to as saturated asymptotic approximations. The given computations support the idea of the instability of steady solutions to the Sivashinsky equation in large domains through huge linear amplification of nonmodal perturbations.

Unlike the presentation of the algorithm is given for a particular equation, the evaluations have been carried out in a very general manner and the algorithm can be straightforwardly applied to a wide variety of nonlinear integro-differential equations.

1 Introduction

Sivashinsky’s equation was obtained in [23] as a weakly nonlinear long wave asymptotic of the Navier-Stokes system combined with the infinite activation energy model of combustion chemistry. The equation governs evolution of the perturbation $\Phi(x_1, x_2, t)$ of the plane flame front moving in the x_3 -direction with the laminar flame speed u_b . Thus, at a given instant of time t , the surface of the flame front is described as $x_3 = t + \Phi(x_1, x_2, t)$, where space coordinates are measured in units of the flame front width δ_{th} and time is in units of δ_{th}/u_b . In these notations, the Sivashinsky equation can be written as follows:

$$\begin{aligned} \frac{\partial \Phi}{\partial t} - \frac{1}{2} \left[\left(\frac{\partial \Phi}{\partial x_1} \right)^2 + \left(\frac{\partial \Phi}{\partial x_2} \right)^2 \right] &= \frac{\partial^2 \Phi}{\partial x_1^2} + \frac{\partial^2 \Phi}{\partial x_2^2} \\ - \frac{\gamma}{4\pi} \left(\frac{\partial^2}{\partial x_1^2} + \frac{\partial^2}{\partial x_2^2} \right) \int_{\mathbf{R}^2} \frac{\Phi(y_1, y_2, t) dy_1 dy_2}{\sqrt{(x_1 - y_1)^2 + (x_2 - y_2)^2}}, & \quad (x_1, x_2) \in \mathbf{R}^2. \end{aligned} \quad (1)$$

It was assumed in the derivation of (1) that the wavelengths of the perturbations are much greater than the width of the flame front. Therefore, the flame front can be considered as a surface separating combustible mixture of density ρ_u and burnt gases of density ρ_b . An assumption of low expansion rate $\rho_b/\rho_u \approx 1$ was also used in order to justify the appearance of the nonlinearity in (1), where the parameter $\gamma = 1 - \rho_b/\rho_u$. Eventually, its weak nonlinearity means that $|\nabla \Phi|$ is assumed to be small.

Because of the asymptotic origins of equation (1), see [24], it cannot be used to model thermal-diffusive instabilities which may occur for sufficiently small values of Lewis number. The proper model to treat this kind of instabilities was also obtained in [23] and is called Kuramoto-Sivashinsky equation.

Physically, equation (1) governs uniform propagation of the flame front along the normal to its surface with the speed u_b affected by the Landau-Darrieus instability [10], [11].

Equation (1) can be written as $\Phi_t - 2^{-1}|\nabla\Phi|^2 = \Delta\Phi + 2^{-1}\gamma(-\Delta)^{1/2}\Phi$ and is reduced in one dimension to

$$\frac{\partial\Phi}{\partial t} - \frac{1}{2}\left(\frac{\partial\Phi}{\partial x}\right)^2 = \frac{\partial^2\Phi}{\partial x^2} + \frac{\gamma}{2}\frac{\partial\mathcal{H}[\Phi]}{\partial x}, \quad x \in \mathbf{R}, \quad (2)$$

where $\mathcal{H}[\Phi] = \pi^{-1} \int_{-\infty}^{\infty} (x-y)^{-1}\Phi(y,t)dy$ is the Hilbert transform. Note, that if $\Phi_1(x,t)$ is an L_1 -periodic solution to (2) for $\gamma = \gamma_1$, then

$$\Phi_2(x,t) = \Phi_1\left(\frac{L_1}{L_2}x, \frac{\gamma_2 L_1}{\gamma_1 L_2}t\right) \quad (3)$$

is an L_2 -periodic solution to (2) for $\gamma = \gamma_2$ if $\gamma_1 L_1 = \gamma_2 L_2$.

A wide class of periodic solutions to (2) was obtained in [25] by using the pole decomposition technique. Namely, it was shown that

$$\Phi(x,t) = \frac{2\pi N_p}{L} \left(\gamma - \frac{4\pi N_p}{L} \right) t + 2 \sum_{n=1}^{N_p} \ln \left| \cosh \left[\frac{2\pi}{L} b_n(t) \right] - \cos \left\{ \frac{2\pi}{L} [x - a_n(t)] \right\} \right| \quad (4)$$

is an L -periodic solution to (2) if

$$\left. \begin{aligned} \frac{da_n}{dt} &= -\frac{2\pi}{L} \sum_{m=1}^{N_p'} \left\{ \frac{\sin[2\pi(a_n - a_m)/L]}{\cosh[2\pi(b_n - b_m)/L] - \cos[2\pi(a_n - a_m)/L]} \right. \\ &\quad \left. + \frac{\sin[2\pi(a_n - a_m)/L]}{\cosh[2\pi(b_n + b_m)/L] - \cos[2\pi(a_n - a_m)/L]} \right\}, \\ \frac{db_n}{dt} &= \frac{2\pi}{L} \coth\left(\frac{2\pi}{L}b_n\right) - \frac{\gamma}{2}\text{sign}b_n \\ &\quad + \frac{2\pi}{L} \sum_{m=1}^{N_p'} \left\{ \frac{\sinh[2\pi(b_n - b_m)/L]}{\cosh[2\pi(b_n - b_m)/L] - \cos[2\pi(a_n - a_m)/L]} \right. \\ &\quad \left. + \frac{\sinh[2\pi(b_n + b_m)/L]}{\cosh[2\pi(b_n + b_m)/L] - \cos[2\pi(a_n - a_m)/L]} \right\}. \end{aligned} \right\} \quad (5)$$

Here N_p is an arbitrary positive integer, and prime in the symbol of summation means $m \neq n$. At every moment of time t , complex numbers $z_n(t) = a_n(t) \pm b_n(t)$, $n = 1, \dots, N_p$ are poles of function (4) and, correspondingly, (4) is called N_p -pole solution of (2). If all the poles in (5) are steady and $a_n = a \in \mathbf{R}$ for $n = 1, \dots, N_p$, then, (4) is called a steady coalescent N_p -pole solution. Solutions of the latter type, denoted here as $\Phi_{N_p}(x)$ and illustrated in Figure 1, have been found to be the strongest attractors of (2). It was shown, see for example [22], that for given period L the number of poles in steady coalescent pole solution (4) may not exceed $N_{p,L} = \text{ceil}(\gamma L/8\pi + 1/2) - 1$, where $\text{ceil}(x)$ is the smallest integer greater or equal to x .

In accordance with the Rayleigh Principia, one would expect that the period L of (5), preferred by (2), is close to the wavelength of the harmonic which is mostly amplified in the linear approximation. This wavelength is equal to $8\pi/\gamma$. However, direct numerical experiments had revealed that the period L preferred by (2) coincides with the size of

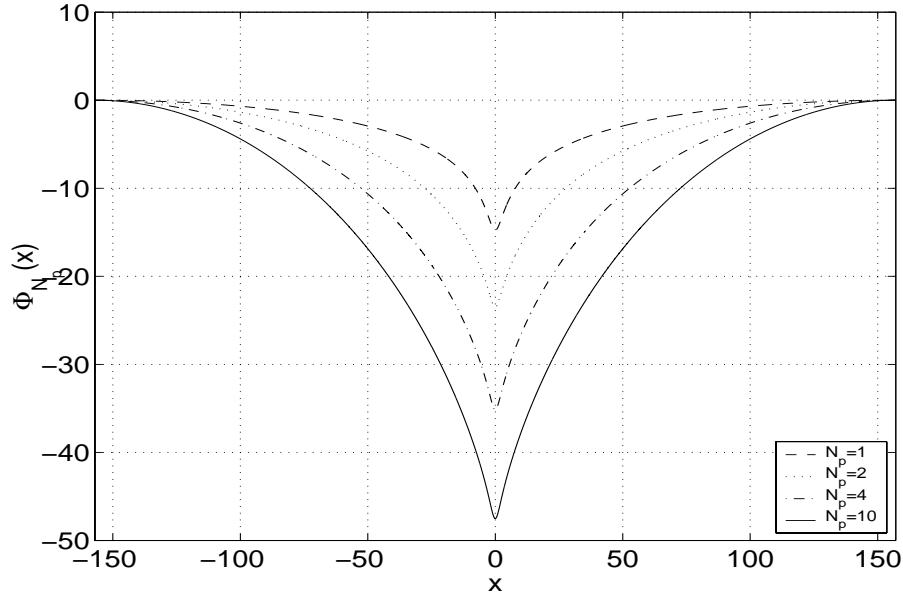


Figure 1: Steady coalescent N_p -pole solutions to the Sivashinsky equation. Here $\gamma = 0.8$ and $L = 100\pi$ ($N_{p,L} = 10$). Graphs have been shifted vertically in order to get $\Phi_{N_p}(\pm L/2) = 0$.

the whole computational domain $[-L/2, L/2]$. Also, the experiments have shown that for sufficiently small values of $L < L_c$ the preferred number of poles is equal $N_{p,L}$. Surprisingly, for larger computational domains $L > L_c$, numerical solutions to (2) do not stabilize to any steady coalescent N_p -pole solution at all. Instead, being essentially nonsteady, they remain very closely to the steady coalescent $N_{p,L}$ -pole solution, developing on the surface of the flame front small cusps arbitrary in time and space [22]. With time these small cusps move towards the trough of the flame front profile and disappear in it as this is shown in Figure 2.

The high sensitivity of pole solutions to certain perturbations was suggested in [6] as an explanation of the cardinal change in the behaviour of numerical solutions to (2) which takes place for $L = L_c$. The argument of [6] was based on a particular asymptotic solution of an approximation to the Sivashinsky equation linearized on the steady coalescent $N_{p,L}$ -pole solution. In the following works [3], [4], and [2], the approach has been developed further and a model equation with stochastic right hand side, explicitly representing the external noise, has been proposed and investigated. Similar conclusions on high sensitivity of the Sivashinsky equation to the external noise have been made in [18] and an estimation of dependence between L_c and the level of the round-off errors has been obtained in [7] in a series of direct numerical simulations.

The eigenvalue analysis of the Sivashinsky equation linearized in a neighbourhood of the steady coalescent pole solution was carried out both numerically [18] and analytically [27]. In both cases the authors concluded that for any $L > 0$ the steady coalescent $N_{p,L}$ -pole solution is the only steady coalescent N_p -pole solution to (2) with all the eigenvalues located in the left half of the complex plane. However, the arguments in support of the assertion were not rigorous enough and, strictly speaking, there is a possibility that eigenvalues in the right half of the complex plane do exist for large values of L even for $\Phi_{N_p,L}(x, t)$. The

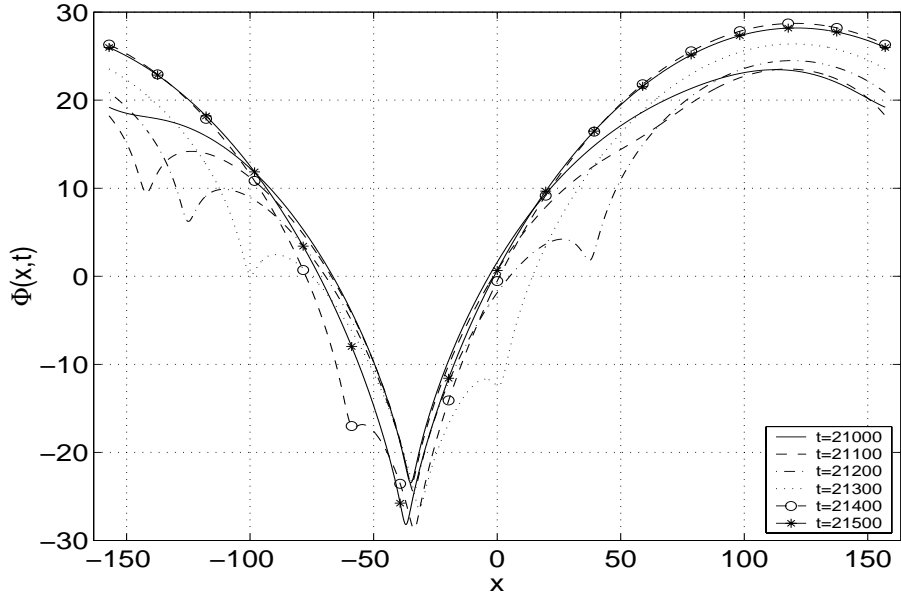


Figure 2: Appearance of small cusps on the surface of the flame front for $\gamma = 0.8$ and $L = 100\pi$.

existence of a chaotic attractor in the Sivashinsky equation cannot be denied as well. In this work we conducted an intensive computational analysis of the Sivashinsky equation to investigate which of the effects listed above is the most likely reason for numerical solutions to (2) not to stabilize to $\Phi_{N_p,L}(x,t)$.

Numerical investigation of stability of steady coalescent $N_{p,L}$ -pole solutions of (2) requires an efficient and high accurate computational algorithm. Taking into account that most of previous numerical studies of (2), see e.g. [15], [5], [2], [4], [18], [21], and [22] were based on spectral methods, it is reasonable to try an essentially different approach with a dissimilar approximation residual. In this work we present such an algorithm based on "approximate approximations" [12], which are known also as saturated asymptotic approximations. The algorithm in question is a natural development of the approach proposed in [8], [9] targeted here at periodic solutions.

The method of "approximate approximations" provides high order approximations of sufficiently smooth functions up to certain prescribed accuracy. Consider for example the approximation of $g(x)$ by the formula

$$g(x) \approx g_h(x) = \frac{1}{\sqrt{D}} \sum_{m=-\infty}^{\infty} g_m \eta_{\mathcal{N}}\left(\frac{x - mh}{\sqrt{D}h}\right), \quad x \in \mathbf{R}. \quad (6)$$

with $g_m = g(hm)$. Here $\eta_{\mathcal{N}}(x)$ is a smooth and rapidly decaying basis function, satisfying the moment condition

$$\int_{-\infty}^{\infty} \eta_{\mathcal{N}}(x) dx = 1, \quad \int_{-\infty}^{\infty} x^n \eta_{\mathcal{N}}(x) dx = 0, \quad n = 1, \dots, N-1.$$

Then for any $\varepsilon > 0$ there exists $D > 0$ that

$$|g(x) - g_h(x)| \leq c_\eta (\sqrt{D}h)^{\mathcal{N}} \|g^{(\mathcal{N})}\|_{L_\infty} + \varepsilon \sum_{n=0}^{\mathcal{N}-1} (\sqrt{D}h)^n |g^{(n)}(x)|$$

(cf. [13]). An example of a suitable basis function is given by

$$\eta_{\mathcal{N}}(x) = \eta_{2\mathcal{N}+2}(x) = e_N \left(-\frac{1}{4} \frac{d^2}{dx^2} \right) \frac{e^{-x^2}}{\sqrt{\pi}} \frac{(-1)^{\mathcal{N}} e^{-x^2}}{\sqrt{\pi} 2^{2\mathcal{N}+1} \mathcal{N}!} \frac{H_{2\mathcal{N}+1}(x)}{x} \quad (7)$$

where $e_N(x) = \sum_{k=0}^N x^k/k!$ is the truncated exponent function, and $H_n(x)$ denotes the Hermite polynomial of order n . The function (7) is not a unique possible basis, but just a choice of many others [14]. Note that formula (6) allows straightforward generalizations to the multivariate case.

Formula (6) with (7) provides approximation of order $O(h^{2\mathcal{N}+2})$ plus a small saturation term $\varepsilon = O(e^{-\pi^2 D})$, see [12]. This term does not disappear when $h \rightarrow 0$, instead it vanishes as $D \rightarrow \infty$. In particular, it can be made less than machine zero ε_M of the computer used in calculations, and, normally, does not produce errors greater than the machine zero does. The accuracy of the ‘‘approximate approximations’’ (6), (7) is limited only by the smoothness of approximated solutions and by the number of the vanishing moments of the basis function. On the other hand, it is only degraded locally if the smoothness of the approximated function is lost locally. The latter property of the method can be especially beneficial for bifurcating solutions with smoothness degrading at the moments of bifurcations.

In Section 2 we develop the algorithm for Sivashinsky’s equation in one spatial dimension, and, in Section 3, the algorithm is extended to the two-dimensional case. In Section 4 we present results of numerical simulations for both one- and two-dimensional equations (2) and (1). These computations indicate that the non-stabilization of numerical solutions in large enough computational domains is of numerical origins and that the small cusps appearing on the flame surface for $L > L_c$ are generated by the round-off errors. Conclusions are given in Section 5.

2 Computational algorithm in one dimension

2.1 Discretization in time

We approximate the one-dimensional equation (2) in time as follows:

$$\begin{aligned} \frac{\Phi^{(n+1)} - \Phi^{(n)}}{\Delta t} &= \sigma_1 \mathcal{L}\Phi^{(n+1)} + (1 - \sigma_1) \mathcal{L}\Phi^{(n)} \\ &+ \frac{\sigma_1}{2} \left(\frac{\partial \Phi}{\partial x} \right)_{t=t_{n+1}}^2 + \frac{\sigma_2}{2} \left(\frac{\partial \Phi}{\partial x} \right)_{t=t_n}^2 + \frac{1 - \sigma_1 - \sigma_2}{2} \left(\frac{\partial \Phi}{\partial x} \right)_{t=t_{n-1}}^2. \end{aligned} \quad (8)$$

Here \mathcal{L} is the pseudodifferential operator composed of linear terms of the Sivashinsky equation

$$\mathcal{L}\Phi = \frac{\partial^2 \Phi}{\partial x^2} + \frac{\gamma}{2} \frac{\partial \mathcal{H}[\Phi]}{\partial x}, \quad (9)$$

and $\Phi^{(n)} = \Phi(x, n\Delta t)$, $n = 0, 1, \dots$. The three time-layer interpolation of the nonlinear term provides a possibility to obtain approximations of second order explicitly. Variable time steps can be used in (8) as well subject to proper modification of the time interpolation in the right hand side. Unlike the variety of available choices for weight coefficients, two major cases of (8) with $\sigma_I = \sigma_1 = \sigma_2 = 1/2$, and $\sigma_I = 1/2$, $\sigma_1 = 0$, $\sigma_2 = 3/4$ have been tested in practice.

Linearizing $(\partial\Phi/\partial x)_{t=t_{n+1}}^2$ in (8) with respect to $\Delta\Phi = \Phi^{(n+1)} - \Phi^{(n)}$ for $\Phi = \Phi^{(n)}$, one obtains

$$\left[I - \Delta t \sigma_I \mathcal{L} - \Delta t \sigma_1 \frac{\partial\Phi^{(n)}}{\partial x} \frac{\partial}{\partial x} \right] \frac{\Phi^{(n+1)} - \Phi^{(n)}}{\Delta t} = \mathcal{L}\Phi^{(n)} + G^{(n)}, \quad (10)$$

where

$$G^{(n)} = \frac{\sigma_1 + \sigma_2}{2} \left(\frac{\partial\Phi}{\partial x} \right)_{t=t_n}^2 + \frac{1 - \sigma_1 - \sigma_2}{2} \left(\frac{\partial\Phi}{\partial x} \right)_{t=t_{n-1}}^2, \quad (11)$$

and I is the identity operator. The approximate factorization of (10) yields

$$(I - \Delta t \sigma_I \mathcal{L}) \left[I - \Delta t \sigma_1 \frac{\partial\Phi^{(n)}}{\partial x} \frac{\partial}{\partial x} \right] \frac{\Phi^{(n+1)} - \Phi^{(n)}}{\Delta t} = \mathcal{L}\Phi^{(n)} + G^{(n)}.$$

Alternatively, equation (10) could be split into fractional time steps.

The factorized equation is solved in two stages, first relatively to $Y^{(n)}$:

$$(I - \Delta t \sigma_I \mathcal{L}) Y^{(n)} = \mathcal{L}\Phi^{(n)} + G^{(n)}, \quad (12)$$

and then relatively to $(\Phi^{(n+1)} - \Phi^{(n)})/\Delta t$:

$$\left[I - \Delta t \sigma_1 \frac{\partial\Phi^{(n)}}{\partial x} \frac{\partial}{\partial x} \right] \frac{\Phi^{(n+1)} - \Phi^{(n)}}{\Delta t} = Y^{(n)}. \quad (13)$$

After a finite difference approximation of $\partial\Phi^{(n)}/\partial x$ and $\partial/\partial x$, the solution of (13) is straightforward, if $\sigma_1 \neq 0$ and is not required at all otherwise. For example, forward and backward sweeps of LU decomposition can be used. The operator $\partial/\partial x$ in (13) has been approximated by central finite-differences of the second order. However, central finite-difference approximations of up to the 8th order have been tested for spatial derivatives $\partial\Phi/\partial x$ in (13) and (11).

In terms of the Fourier transform $\mathcal{F}[f](\xi) = \int_{-\infty}^{\infty} f(x) e^{-i2\pi\xi x} dx$ the solution to (12) can be written as follows

$$\begin{aligned} Y^{(n)}(x) &= (I - \Delta t \sigma_I \mathcal{L})^{-1} (\mathcal{L}\Phi^{(n)} + G^{(n)}) \\ &= \int_{-\infty}^{\infty} \frac{\mathcal{F}[\mathcal{L}](\xi) \mathcal{F}[\Phi^{(n)}](\xi) + \mathcal{F}[G^{(n)}](\xi)}{1 - \Delta t \sigma_I \mathcal{F}[\mathcal{L}](\xi)} e^{i2\pi\xi x} d\xi. \end{aligned} \quad (14)$$

where $\mathcal{F}[\mathcal{L}](\xi) = -4\pi^2\xi^2 + \pi\gamma|\xi|$ is the Fourier image of (9). The evaluation of the Fourier integral (14) is one of the major components of the computational algorithm in question.

2.2 Inversion of the integral operator by using “approximate approximations”

A standard way of calculating the Fourier transform and, eventually, the integral (14), is to approximate the integrand by a series expansion with respect to a set of relatively simple basis functions. Then, the calculation of the Fourier transform of an arbitrary function will be reduced to the evaluation of the Fourier images of the basis functions. In sequel, the calculation of the value of the operator $(I - \Delta t \sigma_I \mathcal{L})^{-1}$ on $\mathcal{L}\Phi^{(n)} + G^{(n)}$, for arbitrary functions $\Phi^{(n)}$ and $G^{(n)}$, will be reduced to evaluating its values on the basis functions. In this work “approximate approximation” is used in order to approximate $\Phi^{(n)}(x)$ and $G^{(n)}(x)$.

It is easy to see that expansion (6), (7) preserves parity of the approximated function. Really, if $g(-x) = \pm g(x)$, $x \in \mathbf{R}$, then $g_h(-x) = \sum_{m=-\infty}^{\infty} g_m \eta_{\mathcal{N}}(-x - mh) = \sum_{m=-\infty}^{\infty} g_m \eta_{\mathcal{N}}(x + mh)$, because $\eta_{\mathcal{N}}(x)$ from (7) is an even function. By introducing a new index $n = -m$, we have $g_h(-x) = \sum_{n=-\infty}^{\infty} g_{-n} \eta_{\mathcal{N}}(x - nh) = \pm \sum_{n=-\infty}^{\infty} g_n \eta_{\mathcal{N}}(x - nh)$, or $g_h(-x) = \pm g_h(x)$.

Also, “approximate approximation” (6) retains periodicity of the approximated function if the period $X \in \mathbf{R}$ is commensurable with the parameter of approximation h . Really, one may write $g_h(x + X) = \sum_{m=-\infty}^{\infty} g_m \eta_{\mathcal{N}}(x + X - mh) = \sum_{m=-\infty}^{\infty} g_m \eta_{\mathcal{N}}[x - (mh - X)]$. Assuming that $X/h = M_X$ is an integer and introducing a new index $n = m - M_X$, we have $g_h(x + X) = \sum_{n=-\infty}^{\infty} g_{n+M_X} \eta_{\mathcal{N}}(x - nh) = \sum_{n=-\infty}^{\infty} g_n \eta_{\mathcal{N}}(x - nh)$, because $g_{n+M_X} = g(nh + M_X h) = g(nh + X) = g(nh) = g_n$. Thus $g_h(x + X) = g_h(x)$ for $X/h \in \mathbf{Z}$.

Application of the Fourier transform to (6), (7) yields

$$\mathcal{F}[g](\xi) \approx \mathcal{F}[g_h](\xi) = \sum_{m=-\infty}^{\infty} g_m \mathcal{F}[\eta_{\mathcal{N}}(x - mh)](\xi), \quad (15)$$

where $\mathcal{F}[\eta_{\mathcal{N}}(x - mh)](\xi) = h e_N(\pi^2 D h^2 \xi^2) e^{-\pi^2 D h^2 \xi^2 - i 2\pi m h \xi}$. Use of (15) in (14) results in the convolution

$$Y_k^{(n)} = \sum_{m=-\infty}^{\infty} C_{k-m}^{(1)} \Phi_m^{(n)} + C_{k-m}^{(2)} G_m^{(n)}, \quad k \in \mathbf{Z}, \quad (16)$$

with coefficients $C_l^{(j)}$, $j = 1, 2$ given by formulas

$$C_l^{(1)} = 2h \int_0^{\infty} \frac{\mathcal{F}[\mathcal{L}](\xi) e_N(\pi^2 D h^2 \xi^2) e^{-\pi^2 D h^2 \xi^2} \cos 2\pi h l \xi}{1 - \Delta t \sigma_I \mathcal{F}[\mathcal{L}](\xi)} d\xi, \quad l \in \mathbf{Z}, \quad (17)$$

$$C_l^{(2)} = 2h \int_0^{\infty} \frac{e_N(\pi^2 D h^2 \xi^2) e^{-\pi^2 D h^2 \xi^2} \cos 2\pi h l \xi}{1 - \Delta t \sigma_I \mathcal{F}[\mathcal{L}](\xi)} d\xi \quad l \in \mathbf{Z}. \quad (18)$$

Note, that $C_l^{(1)} = (\sigma_I \Delta t)^{-1} [C_l^{(2)} - \eta_{\mathcal{N}}(lh)]$ for $l \in \mathbf{Z}$, and the following parity symmetries are held:

$$C_{-l}^{(j)} = C_l^{(j)}, \quad j = 1, 2, \quad l \in \mathbf{Z}. \quad (19)$$

2.3 Discrete convolutions

Considering space periodic solutions and assuming that their period L is comeasurable with the discretization parameter h , i.e. $L/h = 2M \in \mathbf{Z}$, we have $\Phi_m^{(n)} = \Phi_{m+2M}^{(n)}$, $G_m^{(n)} = G_{m+2M}^{(n)}$ for $m \in \mathbf{Z}$. Here, use of an even number for L/h is not a restriction. All the following results take place for odd values of L/h either, but formulas and programming are more complex.

Under assumption of L -periodicity, formula (16) can be transformed into

$$\begin{aligned} Y_k &= \sum_{m=k-M}^{k+M-1} \left[\left(\sum_{l=-\infty}^{\infty} C_{k-m-2lM}^{(1)} \right) \Phi_m^{(n)} + \left(\sum_{l=-\infty}^{\infty} C_{k-m-2lM}^{(2)} \right) G_m^{(n)} \right] \\ &= \sum_{m=k-M}^{k+M-1} B_{k-m}^{(1,M)} \Phi_m^{(n)} + B_{k-m}^{(2,M)} G_m^{(n)}, \quad k = -M, \dots, M-1, \end{aligned} \quad (20)$$

where

$$\begin{aligned} B_l^{(j,M)} &= \sum_{\mu=-\infty}^{\infty} C_{l-2\mu M}^{(j)} = C_l^{(j)} + \sum_{\mu=1}^{\infty} (C_{l-2\mu M}^{(j)} + C_{l+2\mu M}^{(j)}) \\ &= C_l^{(j)} + \sum_{\mu=1}^{\infty} (C_{2\mu M+l}^{(j)} + C_{2\mu M-l}^{(j)}), \quad j = 1, 2, \quad l = -M+1, \dots, M, \end{aligned} \quad (21)$$

because of (19). Functions $\Phi_m^{(n)}$ and $G_m^{(n)}$ are involved in (20) for $m = -2M, \dots, 2M-2$.

Note, that because of the parity of coefficients $C_l^{(j)}$, see (19), coefficients $B_l^{(j,M)}$ hold similar symmetry:

$$B_{-l}^{(j,M)} = B_l^{(j,M)}, \quad j = 1, 2, \quad l = 1, \dots, M-1, \quad (22)$$

and, again, we may consider non-negative values of index l only.

Let us extend $B_l^{(j,M)}$, $j = 1, 2$ for $l = -M, \dots, -2M - m_0 + 2$ and $l = M+1, \dots, 2M$ as zeros and assume that they are $(4M + m_0 - 1)$ -periodic beyond the specified range of values of l . The extended coefficients will be denoted as $A_l^{(j,M)}$. By definition, for $j = 1, 2$,

$$A_l^{(j,M)} = \begin{cases} B_l^{(j,M)} & \text{for } l = -M+1, \dots, M, \\ 0 & \text{for } l = -2M - m_0 + 2, \dots, -M, \\ & l = M+1, \dots, 2M, \end{cases}$$

and

$$A_{l+\nu(4M+m_0-1)}^{(j,M)} = A_l^{(j,M)}, \quad l = -2M - m_0 + 2, \dots, 2M, \quad \nu \in \mathbf{Z} \setminus \{0\}.$$

Here the integer $m_0 \geq 0$ is a parameter regulating the period of extended coefficients $A_l^{(j,M)}$. The value $m_0 = 1$ results in $4M$ -periodicity and is especially convenient for further applications of FFT if M is an integer power of 2.

Generally speaking, this extension of $B_l^{(j,M)}$ no longer possesses symmetry (22) for $l > M-1$, see Figure 3. Namely, for any odd integer μ we may have $A_{-\mu M}^{(j,M)} \neq A_{\mu M}^{(j,M)}$, $j = 1, 2$. However, with this extension, formula

$$Z_k^{(n)} = \sum_{m=-2M}^{2M+m_0-2} A_{k-m}^{(1,M)} \Phi_m^{(n)} + A_{k-m}^{(2,M)} G_m^{(n)}, \quad k = -2M, \dots, 2M + m_0 - 2 \quad (23)$$

is a circular convolution and it provides values of $Z_k^{(n)}$ which coincide with $Y_k^{(n)}$ from (20) for $k = -M, \dots, M-1$, i.e.

$$Y_k^{(n)} \equiv Z_k^{(n)}, \quad \text{for } k = -M, \dots, M-1. \quad (24)$$

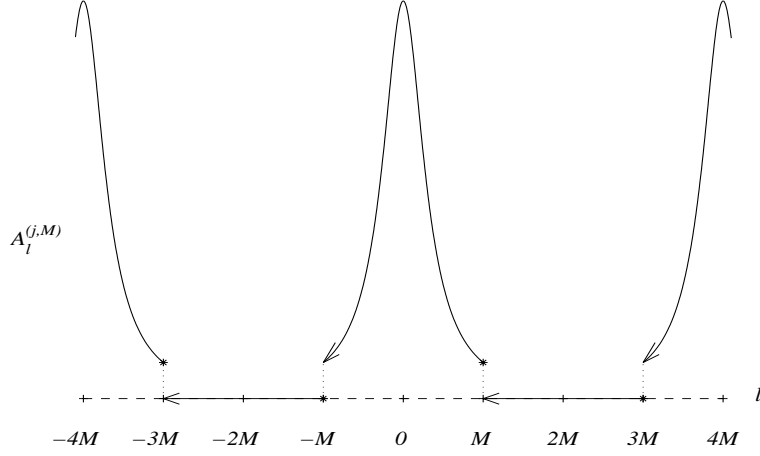


Figure 3: Illustration to the extension of the coefficients $B_l^{(j,M)}$ for $m_0 = 1$, i.e. the period of $A_l^{(j,M)}$ is equal $4M$.

If the discrete Fourier transform $\hat{v}_\kappa = \sum_{k=1}^{4M+m_0-1} v_k e^{-i2\pi \frac{(\kappa-1)(k-1)}{4M+m_0-1}}$, $\kappa = 1, \dots, 4M+m_0-1$ of a sequence $(v_1, v_2, \dots, v_{4M+m_0-1})$ is applied in (23) to the sequences $(A_0^{(j,M)}, A_1^{(j,M)}, \dots, A_{4M+m_0-2}^{(j,M)})$, $(\Phi_{-2M}^{(n)}, \Phi_{-2M+1}^{(n)}, \dots, \Phi_{2M+m_0-2}^{(n)})$ and $(G_{-2M}^{(n)}, G_{-2M+1}^{(n)}, \dots, G_{2M+m_0-2}^{(n)})$, then $\hat{Z}_\kappa^{(n)} = \hat{A}_\kappa^{(1,M)} \hat{\Phi}_\kappa^{(n)} + \hat{A}_\kappa^{(2,M)} \hat{G}_\kappa^{(n)}$, $\kappa = 1, \dots, 4M+m_0-1$. After calculation of these $\hat{Z}_\kappa^{(n)}$, one should use the inverse discrete Fourier transform

$$v_k = (4M+m_0-1)^{-1} \sum_{\kappa=1}^{4M+m_0-1} \hat{v}_\kappa e^{i2\pi \frac{(\kappa-1)(k-1)}{4M+m_0-1}}, \quad k = 1, \dots, 4M+m_0-1,$$

in order to obtain values of $Z_k^{(n)}$, $k = -2M, \dots, 2M+m_0-2$. Only the subset (24) of this sequence corresponding to the main period $k = -M, \dots, M-1$, can be used for retrieving values of $Y_k^{(n)}$.

2.4 Convolution coefficients

The integrands in (17), (18) depend on l through $\cos 2\pi h l \xi$ only. Therefore, after substitution of $C_l^{(j)}$ into (21), a temptation to swap integration and summation may appear. However, the sum

$$\sum_{l=-l_\infty}^{l_\infty} \cos 2\pi h(m-2lM)\xi = \cos 2\pi h m \xi \left[2 \frac{\sin 2\pi h(2l_\infty+1)M\xi}{\sin 2\pi h M \xi} - 1 \right]$$

does not converge as $l_\infty \rightarrow \infty$ and swapping of integration and summation in (21) with (17), (18) is not legal.

The discrete Fourier transform is finite and, certainly, can be swapped with both summation in (21) and integration in (17), (18). However, this neither eases summation (21) nor brings any other benefits.

A better way to tackle the summation in (21) is to use asymptotic expansions of the integrals (17) and (18). Indeed, $C_l^{(j)}$ have the form

$$C_l^{(j)} = 2h \int_0^\infty F_j(\xi) \cos 2\pi h l \xi d\xi, \quad j = 1, 2, \quad (25)$$

where $F_j(\xi)$, $j = 1, 2$, are even functions, rapidly decaying for $\xi \rightarrow \infty$:

$$F_1(\xi) = \frac{\mathcal{F}[\mathcal{L}](\xi) e_N(\pi^2 D h^2 \xi^2) e^{-\pi^2 D h^2 \xi^2}}{1 - \Delta t \sigma_I \mathcal{F}[\mathcal{L}](\xi)}, \quad (26)$$

$$F_2(\xi) = \frac{e_N(\pi^2 D h^2 \xi^2) e^{-\pi^2 D h^2 \xi^2}}{1 - \Delta t \sigma_I \mathcal{F}[\mathcal{L}](\xi)}. \quad (27)$$

Therefore, if l in (25) is large enough, then the Laplace method of asymptotic approximation of the integrals looks very efficient. Really, integration by parts and Lebesgue's theorem yields

$$C_l^{(j)} = 2h \sum_{\kappa=1}^{K_j} \frac{(-1)^\kappa F_j^{(2\kappa-1)}(0)}{(2\pi h l)^{2\kappa}} + O \left[\frac{2h \Delta t F_j^{(2K_j+1)}(0)}{(2\pi h l)^{2K_j+2}} \right], \quad j = 1, 2, \quad (28)$$

where $F_j^{(\kappa)}(0)$ stands for the κ -th derivative of $F_j(\xi)$ for $\xi = 0$.

Splitting the summation in (21) as follows:

$$B_l^{(j,M)} = C_l^{(j)} + \sum_{\mu=-\infty}^{-1} C_{l-2\mu M}^{(j)} + \sum_{\mu=1}^{\infty} C_{l-2\mu M}^{(j)}, \quad j = 1, 2,$$

and substituting asymptotic expansions (28) results in

$$B_l^{(j,M)} = C_l^{(j)} + 2h \sum_{\kappa=1}^{K_j} \frac{(-1)^\kappa F_j^{(2\kappa-1)}(0)}{(4\pi h M)^{2\kappa}} \sum_{\mu=1}^{\infty} \left[\left(\mu + \frac{l}{2M} \right)^{-2\kappa} + \left(\mu - \frac{l}{2M} \right)^{-2\kappa} \right] + O \left\{ \frac{2h F_j^{(2K_j+1)}(0)}{(2\pi h)^{2K_j+2}} \sum_{\mu \in \mathbf{Z} \setminus \{0\}} \frac{1}{(l - 2\mu M)^{2K_j+2}} \right\}, \quad (29)$$

where summations along index μ can now be represented in terms of the polygamma functions $\psi^{(\kappa)}(x)$ for $l \neq 0$:

$$B_l^{(j,M)} = C_l^{(j)} + 2h \sum_{k=1}^{K_j} \frac{(-1)^k F_j^{(2k-1)}(0)}{(4\pi h M)^{2k}} \times \left\{ \frac{(-1)^{2k}}{(2k-1)!} \left[\psi^{(2k-1)} \left(\frac{l}{2M} \right) + \psi^{(2k-1)} \left(-\frac{l}{2M} \right) \right] - 2 \left(\frac{2M}{l} \right)^{2k} \right\}$$

$$+O \left\{ \frac{2hF_j^{(2K_j+1)}(0)}{(2\pi h)^{2K_j+2}} \sum_{\mu \in \mathbf{Z} \setminus \{0\}} \frac{1}{(l - 2\mu M)^{2K_j+2}} \right\}.$$

Further, using the $(2\kappa - 1)$ -th derivative of the symmetry relationship $\psi(x) - \psi(-x) = -\pi \cot \pi x - x^{-1}$, see p. 774 in [19], together with the representation of $\alpha^{-2\kappa}$ as the $(2\kappa - 1)$ -th derivative of α^{-1} , yields the required formula:

$$B_l^{(j,M)} = C_l^{(j)} + 2h \sum_{\kappa=1}^{K_j} \frac{(-1)^{\kappa-1} F_j^{(2\kappa-1)}(0)}{(4hM)^{2\kappa} (2\kappa - 1)!} \left. \frac{d^{2\kappa-1} \cot \alpha - \alpha^{-1}}{d\alpha^{2\kappa-1}} \right|_{\alpha=\frac{\pi l}{2M}} \\ + O \left[\frac{6hF_j^{(2K_j+1)}(0)}{(2\pi hM)^{2K_j+2}} \right], \quad l = -M + 1, \dots, -1, 1, \dots, M, \quad j = 1, 2, \quad (30)$$

where an estimation of the expansion error is carried out in the Appendix 7.1.

In the case $l = 0$, we rewrite (29) as follows:

$$B_0^{(j,M)} = C_0^{(j)} + 2h \sum_{\kappa=1}^{K_j} \frac{(-1)^\kappa F_j^{(2\kappa-1)}(0)}{(4\pi hM)^{2\kappa}} \left(\sum_{\mu \in \mathbf{Z} \setminus \{0\}} \mu^{-2\kappa} \right) \\ + O \left\{ \frac{2hF_j^{(2K_j+1)}(0)}{(4\pi hM)^{2K_j+2}} \left(\sum_{\mu \in \mathbf{Z} \setminus \{0\}} \mu^{-2K_j-2} \right) \right\}.$$

By making use of the Riemann zeta function, the last formula takes the form

$$B_0^{(j,M)} = C_0^{(j)} + 4h \sum_{\kappa=1}^{K_j} \frac{(-1)^\kappa F_j^{(2\kappa-1)}(0)}{(4\pi hM)^{2\kappa}} \zeta(2\kappa) + O \left\{ \frac{8hF_j^{(2K_j+1)}(0)}{(4\pi hM)^{2K_j+2}} \right\}, \quad (31)$$

because, (see (74) and (75) in the Appendix), $|\zeta(2K_j + 2)| < \frac{2^{2K_j+1}}{2^{2K_j+1}-1} \leq 2$. Note, that (31) involves values of Riemann's zeta function for even and positive integers only.

For coefficients $B_l^{(j,M)}$ the error of the asymptotic expansions was estimated in (30) for $l = -M + 1, \dots, -1, 1, \dots, M$:

$$E_{K_j}^{(j,M)} = O \left[\frac{6h\Delta t F_j^{(2K_j+1)}(0)}{(2\pi hM)^{2K_j+2}} \right], \quad j = 1, 2.$$

It is obviously greater than the error for $l = 0$ given in (31).

Figures 4 and 5 show graphs of $E_{K_2}^{(2,M)}$ versus K_2 for typical values of L and Δt . Values of parameters not mentioned in the legends are $h = 0.01$, $D = 4$, $N = 0$, and $\gamma = 0.8$. Dependence of $E_{K_2}^{(2,M)}$ on h is much weaker and corresponding graphs are not given.

2.5 Crucial aspects of implementation

The accurate calculation of high derivatives of $F_j(\xi)$ for $\xi = 0$ and of $\cot \alpha - \alpha^{-1}$ in (30) and (31) is crucial in the practical implementation of the algorithm.

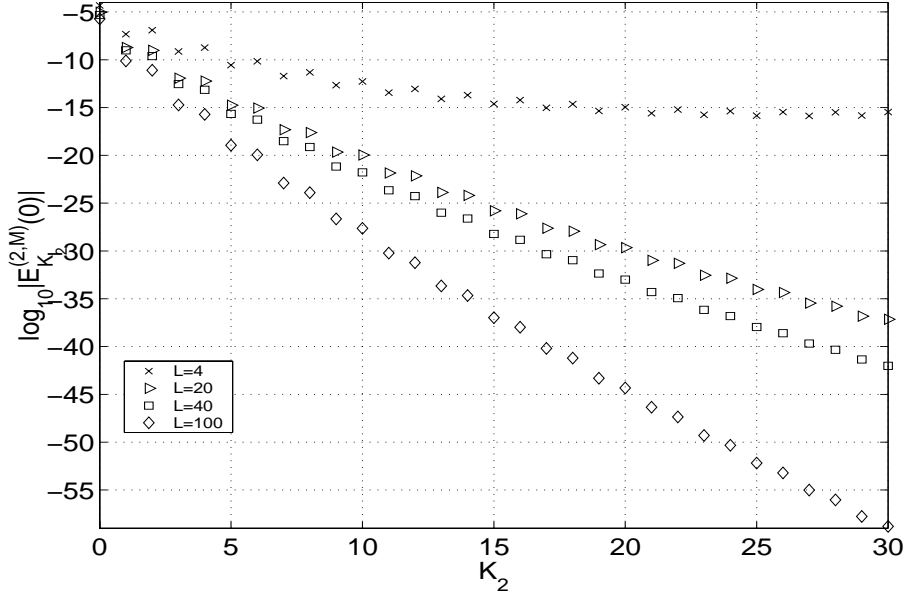


Figure 4: Dependence of $E_{K_2}^{(2,M)}$ on K_2 for a set of values of L ; $\Delta t = 0.01$.

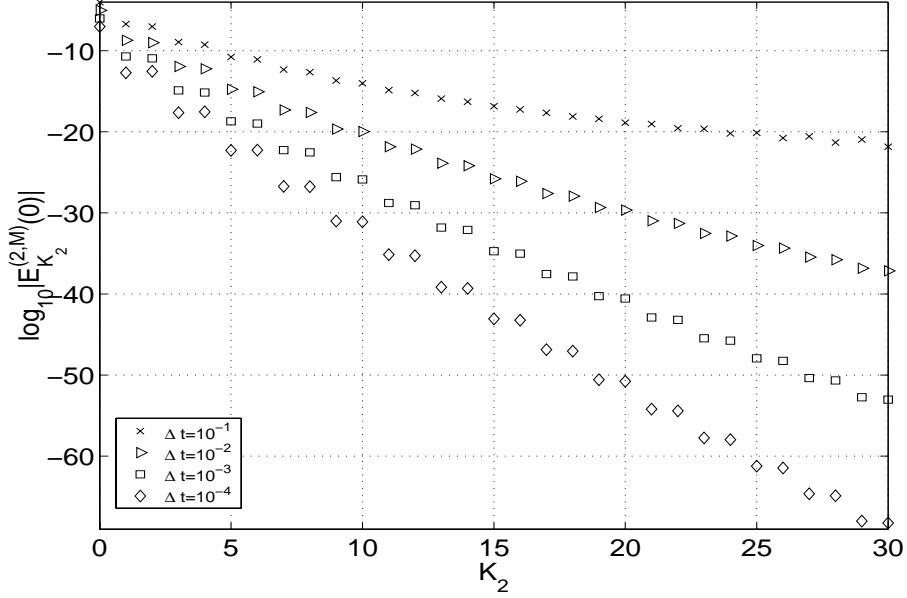


Figure 5: Dependence of $E_{K_2}^{(2,M)}$ on K_2 for a set of values of Δt ; $L = 20$.

Starting from computational formulas for $F_2^{(k)}(0)$, we note that it can be represented as a product of three functions $e_N(\pi^2 D h^2 \xi^2)$, $e^{-\pi^2 D h^2 \xi^2}$, and $1/\mathcal{G}(\xi)$, where

$$\mathcal{G}(\xi) = 1 - \Delta t \sigma_I \mathcal{F}[\mathcal{L}](\xi) = 1 + \Delta t \sigma_I (4\pi^2 \xi^2 - \pi \gamma |\xi|). \quad (32)$$

Thus, the application of the Leibnitz rule reduces the problem to the evaluation of deriva-

tives of arbitrary orders of the factors. It is easy to see that

$$\left. \begin{aligned} \frac{d^{2\mu+1} e_N(\pi^2 D h^2 \xi^2)}{d\xi^{2\mu+1}} \Big|_{\xi=0} &= 0, & \mu = 0, 1, 2, \dots, \\ \frac{d^{2\mu} e_N(\pi^2 D h^2 \xi^2)}{d\xi^{2\mu}} \Big|_{\xi=0} &= \frac{2\mu!}{\mu!} (\pi^2 D h^2)^\mu, & \mu = 0, 1, 2, \dots, N, \\ \frac{d^{2\mu} e_N(\pi^2 D h^2 \xi^2)}{d\xi^{2\mu}} \Big|_{\xi=0} &= 0, & \mu > N, \end{aligned} \right\}$$

and

$$\left. \begin{aligned} \frac{d^{2\mu+1} e^{-\pi^2 D h^2 \xi^2}}{d\xi^{2\mu+1}} \Big|_{\xi=0} &= 0, & \mu = 0, 1, 2, \dots, \\ \frac{d^{2\mu} e^{-\pi^2 D h^2 \xi^2}}{d\xi^{2\mu}} \Big|_{\xi=0} &= \frac{2\mu!}{\mu!} (-\pi^2 D h^2)^\mu, & \mu = 1, 2, 3, \dots \end{aligned} \right\} \quad (33)$$

Values of $\{[\mathcal{G}(\xi)]^{-1}\}^{(\nu)}$ for $\xi = 0$ can be obtained with the help of the expansion $(1-x)^{-1} = 1 + x + x^2 + \dots$, which is valid for $|x| < 1$. Using it for $[\mathcal{G}(\xi)]^{-1}$ in an ε -vicinity of $\xi = 0$ and, further, differentiating the expansion term-by-term, yields for $\xi = 0$

$$\frac{d^\nu [\mathcal{G}(\xi)]^{-1}}{d\xi^\nu} \Big|_{\xi=0} = \nu! \pi^\nu \sum_{\mu=\text{ceil}(\frac{\nu}{2})}^{\nu} \binom{\mu}{2\mu-\nu} (-4)^{\nu-\mu} \gamma^{2\mu-\nu} (\Delta t \sigma_I)^\mu.$$

Figure 6 gives an idea on typical values of $[(\mathcal{G})^{-1}]^{(\nu)}(0)$ as a function of ν for $\gamma = 0.8$, $\sigma_I = 1$, and for a set of different time steps Δt .

Graphs in Fig. 6 show that high order derivatives of $\mathcal{G}^{-1}(\xi)$ for $\xi = 0$ may become very large as their order grows. Fortunately, large values of $\{\mathcal{G}^{-1}(\xi)\}^{(\nu)}$ for $\xi = 0$ are compensated by other factors, and the terms of expansion (30) are eventually decaying as it can be seen from Figs. 4 and 5.

Figure 7 shows the graph of $|F_2^{(\kappa)}(0)|$ versus κ for $h = 0.01$, $D = 4$, $N = 0$, $\gamma = 0.8$, and for a set of Δt . The saw-shape of the graph is explained by the alternation of the odd-even order of the derivatives. The graph itself is point-wise and is defined for integer values of κ only. Similar to high order derivatives of $\mathcal{G}^{-1}(\xi)$, these functions can become very large for large κ as well and certain care is required in practical implementations of (30) in order to avoid severe round-off errors. In our calculations κ did not exceed 12 usually.

Another important parameter is γ . For $\gamma = 0$ all odd derivatives of $F_2^{(\kappa)}(0)$ vanish, making asymptotic expansions of the previous Section senseless and indicating that the convolution coefficients $C_l^{(j)}$ decay exponentially for $l \rightarrow \infty$. This behaviour is explained by the fact that for $\gamma = 0$ equation (2) turns into Burgers' equation and is no longer nonlocal. The effect of γ within the range $0.1 \leq \gamma \leq 1$ and of other parameters on $F_2^{(\kappa)}(0)$ is less pronounced and the corresponding graphs are not shown for the sake of brevity.

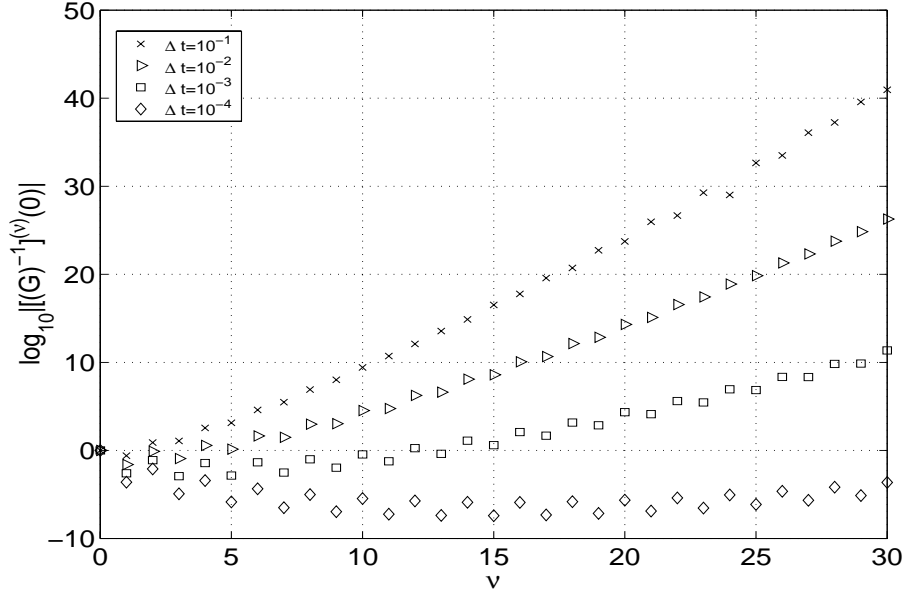


Figure 6: Dependence of $\log_{10} |[(\mathcal{G})^{-1}]^{(\nu)}(0)|$ versus ν for a set of Δt .

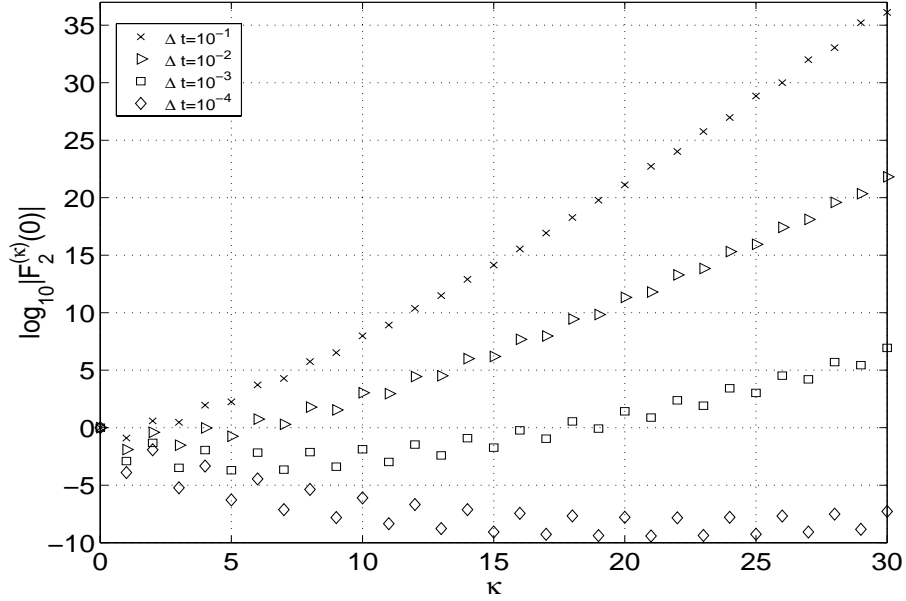


Figure 7: Dependence of $|F_2^{(\kappa)}(0)|$ versus κ for a set of Δt .

The values of $F_1^{(\kappa)}(0)$ can be conveniently expressed in terms of $F_2^{(\kappa)}(0)$:

$$F_1^{(\kappa)}(0) = \begin{cases} \pi\gamma F_2(0), & \kappa = 1, \\ \kappa\pi\gamma F_2^{(\kappa-1)}(0) - 4\kappa(\kappa-1)\pi^2 F_2^{(\kappa-2)}(0), & \kappa = 2, 3, \dots \end{cases}$$

In order to calculate high order derivatives of $\cot \alpha - \alpha^{-1}$, we employ its power series

expansion (see entry 4.3.70, p. 75 of [1] and (74) in the Appendix):

$$\cot \alpha - \alpha^{-1} = -2 \sum_{\mu=1}^{\infty} \frac{\zeta(2\mu)}{\pi^{2\mu}} \alpha^{2\mu-1}, \quad |\alpha| < \pi.$$

After differentiating $2\kappa + 1$ times, $\kappa = 0, 1, 2, \dots$, it takes the form

$$\frac{d^{2\kappa+1} \cot \alpha - \alpha^{-1}}{d\alpha^{2\kappa+1}} = -\frac{2}{\pi^{2\kappa+2}} \sum_{\mu=1}^{\infty} \zeta(2\mu + 2\kappa) \frac{(2\mu + 2\kappa - 1)!}{(2\mu - 2)!} \left(\frac{\alpha}{\pi}\right)^{2\mu-2}. \quad (34)$$

We remind that $\alpha = \pi|l|/2M$, $l = 1, \dots, M$, i.e. $\alpha \leq \pi/2$ and only derivatives of odd order of $\cot \alpha - \alpha^{-1}$ are used in formulas for convolution coefficients.

It should be taken into account in implementations that for sufficiently large κ and α , the summands of (34) reach their maximum for $\mu \approx (\kappa + 1/2)(\pi/\alpha - 1)^{-1} + 1$. Figure 8 illustrates the dependence of (34) on κ for a set of different α .

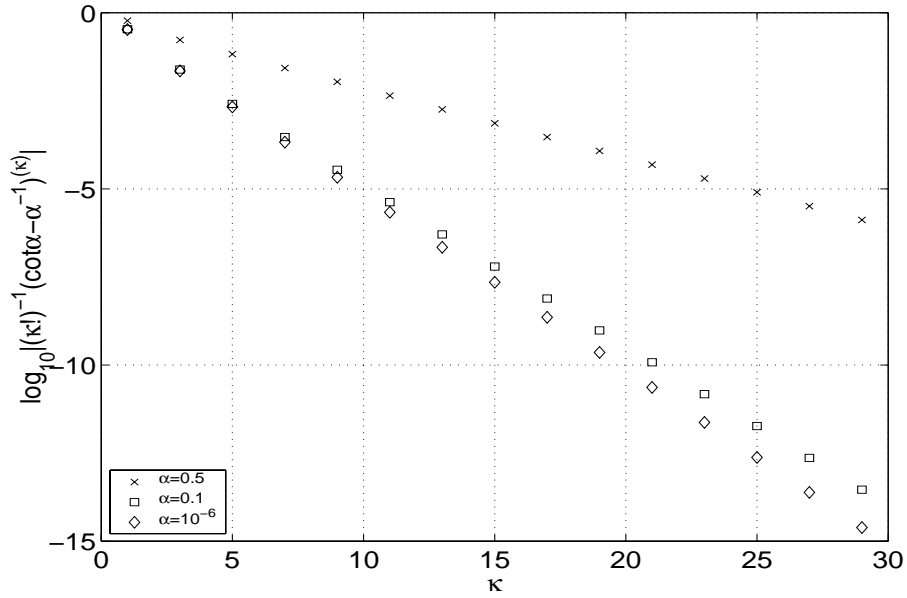


Figure 8: Dependence of $d^\kappa(\cot \alpha - \alpha^{-1})/d\alpha^\kappa$ on κ , calculated by formula (34) for a set of values of α .

The function $d^{2\kappa-1}(\cot \alpha - \alpha^{-1})/d\alpha^{2\kappa-1}$ is just the properly normalized series from (29)

$$\frac{d^{2\kappa-1} \cot \alpha - \alpha^{-1}}{d\alpha^{2\kappa-1}} \propto \sum_{\mu=1}^{\infty} \left[\left(\mu + \frac{\alpha}{\pi}\right)^{-2\kappa} + \left(\mu - \frac{\alpha}{\pi}\right)^{-2\kappa} \right], \quad (35)$$

and a reasonable question arises, whether it would not be easier to calculate $d^{2\kappa-1}(\cot \alpha - \alpha^{-1})/d\alpha^{2\kappa-1}$ directly from (35), once eventually we calculate it by summation of another series. In order to answer the question, we note that the residual of (35) cut off at $\mu = M_\infty$ is of order $M_\infty^{-2\kappa+1}$. This means, in turn, that for $\kappa = 1$ direct summation with accuracy of order 10^{-16} would require to take into account about 10^{16} terms and is practically impossible.

Besides the infinite summation, formula (21) for calculating $B_l^{(j,M)}$ includes the calculation of $C_l^{(j)}$ from (17), (18) for $l = -M + 1, \dots, M$. Because of the fast decay of the integrand, numerical integration is very efficient and can be done by standard routines from QUADPACK [17] or NAG Fortran Library [16]. Unfortunately, the accuracy of these universal algorithms is at most about 3-4 decimal digits less than machine precision. Therefore, in order to reach the accuracy on the level of machine precision, a special tackling of (17), (18) is required. In particular, the function $[\mathcal{G}(\xi)]^{-1}$ from (32) can be approximated by (6), (7) and substituted into (17), (18). The result can be integrated analytically by using [20], p. 452, entry 2.5.36.9. For small enough Δt , when high derivatives of $[\mathcal{G}(\xi)]^{-1}$ are not very large (see Fig. 6), the approximation accuracy of the integrals in (17), (18) can be improved up to the machine zero [13].

Comprehensive data on values of Riemann's zeta function for integer values of the argument are given in Table 23.3, p. 811 of [1].

3 Computational algorithm in two dimensions

3.1 Approximation

By analogy with the one-dimensional case, we split the computations into two stages

$$(I - \Delta t \sigma_I \mathcal{L}) Y^{(n)} = \mathcal{L} \Phi^{(n)} + G^{(n)}, \quad (36)$$

and

$$\left[I - \Delta t \sigma_1 \frac{\partial \Phi^{(n)}}{\partial x_1} \frac{\partial}{\partial x_1} \right] \left[I - \Delta t \sigma_1 \frac{\partial \Phi^{(n)}}{\partial x_2} \frac{\partial}{\partial x_2} \right] \frac{\Phi^{(n+1)} - \Phi^{(n)}}{\Delta t} = Y^{(n)}, \quad (37)$$

where, on this occasion,

$$\begin{aligned} \mathcal{L} \Phi &= \frac{\partial^2 \Phi}{\partial x_1^2} + \frac{\partial^2 \Phi}{\partial x_2^2} - \frac{\gamma}{4\pi} \Delta \int_{\mathbf{R}^2} \frac{\Phi(y_1, y_2, t) d\mathbf{y}}{|\mathbf{x} - \mathbf{y}|}, \\ G^{(n)} &= \frac{\sigma_1 + \sigma_2}{2} \left[\left(\frac{\partial \Phi^{(n)}}{\partial x_1} \right)^2 + \left(\frac{\partial \Phi^{(n)}}{\partial x_2} \right)^2 \right] \\ &+ \frac{1 - \sigma_1 - \sigma_2}{2} \left[\left(\frac{\partial \Phi^{(n-1)}}{\partial x_1} \right)^2 + \left(\frac{\partial \Phi^{(n-1)}}{\partial x_2} \right)^2 \right], \end{aligned}$$

$\mathbf{x} = (x_1, x_2)$, $\mathbf{y} = (y_1, y_2)$, and $\Phi^{(n)} = \Phi(x_1, x_2, n\Delta t)$, $n = 0, 1, \dots$

Again, after a finite difference approximation of space derivatives, the solution to (37) can be obtained by forward and backward sweeps of LU decomposition. The solution to (36) in terms of the Fourier transform is

$$Y^{(n)}(\mathbf{x}) = \int_{\mathbf{R}^2} \frac{\mathcal{F}[\mathcal{L}](\boldsymbol{\xi}) \mathcal{F}[\Phi^{(n)}](\boldsymbol{\xi}) + \mathcal{F}[G^{(n)}](\boldsymbol{\xi})}{1 - \Delta t \sigma_I \mathcal{F}[\mathcal{L}](\boldsymbol{\xi})} e^{i2\pi(\boldsymbol{\xi} \cdot \mathbf{x})} d\boldsymbol{\xi}, \quad (38)$$

where $\mathcal{F}[\mathcal{L}](\boldsymbol{\xi}) = -4\pi^2 |\boldsymbol{\xi}|^2 + \pi\gamma |\boldsymbol{\xi}|$, and $\boldsymbol{\xi} = (\xi_1, \xi_2)$.

The approximation formula (6) in two dimensions takes the form

$$g(\mathbf{x}) \approx g_h(\mathbf{x}) = \frac{1}{D} \sum_{\mathbf{m} \in \mathbf{Z}^2} g_{\mathbf{m}} \eta_{\mathcal{N}}\left(\frac{\mathbf{x} - \mathbf{m}h}{\sqrt{D}h}\right), \quad (39)$$

where $\mathbf{m} = (m_1, m_2)$ and $g_{\mathbf{m}} = g(\mathbf{m}h)$. As basis function one can use

$$\eta_{\mathcal{N}}(\mathbf{x}) = \eta_{2N+2}(\mathbf{x}) = \frac{1}{\pi} e_N\left(-\frac{1}{4}\Delta\right) e^{-|\mathbf{x}|^2} = \frac{e^{-|\mathbf{x}|^2}}{\pi} L_{N+1}^{(1)}(|\mathbf{x}|^2), \quad (40)$$

where

$$L_n^{(1)}(y) = \frac{e^y y^{-1}}{n!} \left(\frac{d}{dy}\right)^n (e^{-y} y^{n+1})$$

is the generalized Laguerre polynomial of order n . Similar to the one-dimensional case, formula (39) with (40) provides approximation of order $O(h^{2N+2})$ plus a small saturation term of order $O(e^{-\pi^2 D})$, see [12], [13].

The Fourier transform of (39) is

$$\mathcal{F}[g](\boldsymbol{\xi}) \approx \mathcal{F}[g_h](\boldsymbol{\xi}) = h^2 e_N(\pi^2 D h^2 |\boldsymbol{\xi}|^2) e^{-\pi^2 D h^2 |\boldsymbol{\xi}|^2} \sum_{\mathbf{m} \in \mathbf{Z}^2} g_{\mathbf{m}} e^{-2\pi i h(\mathbf{m} \cdot \boldsymbol{\xi})} \quad (41)$$

Substitution of (41) into (38) results in the convolution

$$Y_{\mathbf{k}}^{(n)} = \sum_{\mathbf{m} \in \mathbf{Z}^2} C_{\mathbf{k}-\mathbf{m}}^{(1)} \Phi_{\mathbf{m}}^{(n)} + C_{\mathbf{k}-\mathbf{m}}^{(2)} G_{\mathbf{m}}^{(n)}, \quad \mathbf{k} \in \mathbf{Z}^2, \quad (42)$$

with coefficients $C_l^{(j)}$, $j = 1, 2$

$$C_l^{(1)} = 2\pi h^2 \int_0^\infty \frac{\xi \mathcal{F}[\mathcal{L}](\xi) e_N(\pi^2 D h^2 \xi^2) e^{-\pi^2 D h^2 \xi^2} J_0(2\pi h |l| \xi)}{1 - \Delta t \sigma_I \mathcal{F}[\mathcal{L}](\xi)} d\xi, \quad l \in \mathbf{Z}^2, \quad (43)$$

$$C_l^{(2)} = 2\pi h^2 \int_0^\infty \frac{\xi e_N(\pi^2 D h^2 \xi^2) e^{-\pi^2 D h^2 \xi^2} J_0(2\pi h |l| \xi)}{1 - \Delta t \sigma_I \mathcal{F}[\mathcal{L}](\xi)} d\xi, \quad l \in \mathbf{Z}^2, \quad (44)$$

where $J_0(x)$ is the Bessel function of zero order. These coefficients are even functions of both components of index l , and $C_l^{(1)} = (\sigma_I \Delta t)^{-1} [C_l^{(2)} - \eta_{\mathcal{N}}(hl)]$, for $l \in \mathbf{Z}^2$.

Considering space periodic solutions and assuming that their period $\mathbf{L} = (L, L)$ is commensurable with the discretization parameter h , i.e. $L/h = 2M \in \mathbf{Z}$, we have: $\Phi_{\mathbf{m}}^{(n)} = \Phi_{\mathbf{m}+2\mathbf{M}}^{(n)}$, $G_{\mathbf{m}}^{(n)} = G_{\mathbf{m}+2\mathbf{M}}^{(n)}$, $\mathbf{m} \in \mathbf{Z}^2$, where $\mathbf{M} = (M, M)$. Then, formula (42) can be transformed into

$$Y_{\mathbf{k}} = \sum_{m_1=k_1-M}^{k_1+M-1} \sum_{m_2=k_2-M}^{k_2+M-1} B_{\mathbf{k}-\mathbf{m}}^{(1,M)} \Phi_{\mathbf{m}}^{(n)} + B_{\mathbf{k}-\mathbf{m}}^{(2,M)} G_{\mathbf{m}}^{(n)}, \quad -M \leq k_1, k_2 \leq M-1, \quad (45)$$

where

$$B_l^{(j,M)} = \sum_{\boldsymbol{\mu} \in \mathbf{Z}^2} C_{l-2M\boldsymbol{\mu}}^{(j)} = C_l^{(j)} + \sum_{\boldsymbol{\mu} \in \mathbf{Z}^2 \setminus \{\mathbf{0}\}} C_{l-2M\boldsymbol{\mu}}^{(j)}, \quad (46)$$

for $-M + 1 \leq l_1, l_2 \leq M$ and $j = 1, 2$. The functions $\Phi_{\mathbf{m}}^{(n)}$ and $G_{\mathbf{m}}^{(n)}$ are involved in (45) for $-2M \leq m_1, m_2 \leq 2M - 2$.

Note, that coefficients $B_{\mathbf{l}}^{(j,M)}$ hold the same parity in both components of index \mathbf{l} as coefficients $C_{\mathbf{l}}^{(j)}$ do. However, unlike $C_{\mathbf{l}}^{(j)}$, the coefficients $B_{\mathbf{l}}^{(j,M)}$ are no longer radial functions with respect to the index \mathbf{l} .

Now, similarly to the one-dimensional case, we introduce coefficients $A_{\mathbf{l}}^{(j,M)}$ in such a way that $A_{\mathbf{l}}^{(j,M)} = B_{\mathbf{l}}^{(j,M)}$, for $-M + 1 \leq l_1, l_2 \leq M$. Also, $A_{\mathbf{l}}^{(j,M)} = 0$ for $-2M - m_0 + 2 \leq l_1, l_2 \leq 2M$, with at least one of l_1, l_2 is either greater than M or smaller than $-M + 1$. Eventually, values of $A_{\mathbf{l}}^{(j,M)}$ at all other points of \mathbf{Z}^2 are defined by periodicity: $A_{\mathbf{l}+(4M+m_0-1)\boldsymbol{\nu}}^{(j,M)} = A_{\mathbf{l}}^{(j,M)}$, for $-2M - m_0 + 2 \leq l_1, l_2 \leq 2M$, and $\boldsymbol{\nu} \in \mathbf{Z}^2 \setminus \{\mathbf{0}\}$. With this extension, formula

$$Z_{\mathbf{k}}^{(n)} = \sum_{m_1=-2M}^{2M+m_0-2} \sum_{m_2=-2M}^{2M+m_0-2} A_{\mathbf{k}-\mathbf{m}}^{(1,M)} \Phi_{\mathbf{m}}^{(n)} + A_{\mathbf{k}-\mathbf{m}}^{(2,M)} G_{\mathbf{m}}^{(n)}, \quad (47)$$

for $-2M \leq k_1, k_2 \leq 2M + m_0 - 2$ is a two dimensional circular convolution. For $-M \leq k_1, k_2 \leq M - 1$ it provides values of $Z_{\mathbf{k}}^{(n)}$ which coincide with $Y_{\mathbf{k}}^{(n)}$ from (45). Efficient summation in (47) can be carried out with the two dimensional discrete Fourier transform. The transform is directionwise and all the computational formulas follow from the one-dimensional ones straightforwardly.

3.2 Convolution coefficients

In two dimensions the convolution coefficients $C_{\mathbf{l}}^{(j)}$ have a form of Hankel transform of the zero order:

$$C_{\mathbf{l}}^{(j)} = 2\pi h^2 \int_0^{\infty} \xi F_j(\xi) J_0(2\pi h|\mathbf{l}|\xi) d\xi, \quad j = 1, 2, \quad (48)$$

where $F_j(\xi)$, $j = 1, 2$, are exactly the same as in the one-dimensional case, i.e. are given by formulas (26) and (27). Here, for large enough values of $|\mathbf{l}|$, the integrand will frequently oscillate as well, however, the application of the Laplace method of asymptotic approximation of the integral is not straightforward because of the lack of a theorem similar to Lebesgue's one for Fourier integrals.

In order to obtain an asymptotic expansion of (48) for $|\mathbf{l}| \rightarrow \infty$ we consider the integral

$$\int_0^{\infty} Q(\xi) e^{-a\xi^2} J_0(b\xi) d\xi \quad (49)$$

for a sufficiently smooth function $Q(\xi)$ and large $b > 0$. By virtue of the rapid decay of the integrand, we assume that the nonnegligible contribution to the integral comes from a vicinity of $\xi = 0$, where $Q(\xi)$ can be represented by the Taylor series. Then, integral (49) can be approximated by a linear combination of integrals

$$\int_0^{\infty} \xi^n e^{-a\xi^2} J_0(b\xi) d\xi, \quad n = 0, 1, 2, \dots \quad (50)$$

The latter can be written in terms of the confluent hypergeometric function (see entry 2.12.9.3, p. 186 of [20]):

$$\int_0^{\infty} \xi^n e^{-a\xi^2} J_0(b\xi) d\xi = \frac{1}{2} \Gamma\left(\frac{n+1}{2}\right) a^{-\frac{n+1}{2}} {}_1F_1\left(\frac{n+1}{2}; 1; -\frac{b^2}{4a}\right). \quad (51)$$

The asymptotics of ${}_1F_1$ in (51) for $b \rightarrow \infty$ and even $n = 2m$ is given in entry 13.5.1, p. 508 of [1]:

$$\begin{aligned} {}_1F_1\left(m + \frac{1}{2}; 1; -\frac{b^2}{4a}\right) &= \frac{(-1)^m}{\pi \Gamma(m + 1/2)} \sum_{\kappa=0}^K \frac{[\Gamma(m + \kappa + 1/2)]^2 (4a)^{m+\kappa+1/2}}{\kappa! b^{2m+2\kappa+1}} \\ &+ O\left[\frac{(4a)^{m+K+3/2}}{\pi \Gamma(m + 1/2) b^{2m+2K+3}}\right], \end{aligned} \quad (52)$$

where the relation $\Gamma(m + 1/2)\Gamma(1/2 - m) = (-1)^m \pi$ was employed. For odd values of n the asymptotics is exponential and the contribution from corresponding terms into (49) is asymptotically negligible in comparison to (52).

Combining (50)-(52), yields after an appropriate regrouping of summands

$$\begin{aligned} \int_0^{\infty} Q(\xi) e^{-a\xi^2} J_0(b\xi) d\xi &= \sum_{\kappa=0}^K \frac{(-1)^\kappa (2\kappa)!}{(2^\kappa \kappa!)^2 b^{2\kappa+1}} \left. \frac{d^{2\kappa} Q(\xi) e^{-a\xi^2}}{d\xi^{2\kappa}} \right|_{\xi=0} \\ &+ O\left\{ \frac{(2K+2)!}{[2^{K+1}(K+1)!]^2 b^{2K+3}} \left. \frac{d^{2K+2} Q(\xi) e^{-a\xi^2}}{d\xi^{2K+2}} \right|_{\xi=0} \right\} \end{aligned} \quad (53)$$

for $b \rightarrow \infty$. Here we have also used (33) for high order derivatives of $e^{-a\xi^2}$, Leibniz' formula for differentiation of a product of functions and the expression of the gamma function of a half-integer argument in terms of factorial $\Gamma(m + 1/2) = \sqrt{\pi} 2^{-2m} (2m)! / (m)!$. Turning back to (48), we have

$$\begin{aligned} C_l^{(j)} &= 2\pi h^2 \sum_{\kappa=0}^K \frac{(-1)^\kappa (2\kappa)!}{(2^\kappa \kappa!)^2 (2\pi h |l|)^{2\kappa+1}} \left. \frac{d^{2\kappa} \xi F_j(\xi)}{d\xi^{2\kappa}} \right|_{\xi=0} \\ &+ O\left\{ \frac{2\pi h^2 (2K+2)!}{[2^{K+1}(K+1)!]^2 (2\pi h |l|)^{2K+3}} \left. \frac{d^{2K+2} \xi F_j(\xi)}{d\xi^{2K+2}} \right|_{\xi=0} \right\}, \quad j = 1, 2. \end{aligned} \quad (54)$$

One can see that $C_l^{(j)} \sim |l|^{-3}$ for $|l| \rightarrow \infty$ because of $\xi F(\xi)|_{\xi=0} = 0$.

Note, that reiterative integration by parts in a generalization of (49) yields

$$\begin{aligned} \int_0^{\infty} Q(\xi) J_0(b\xi) d\xi &= \sum_{\kappa=0}^K \frac{(-1)^{\kappa+1}}{b^{\kappa+1}} Q^{(\kappa)}(0) J_{0,\kappa+1}(0) \\ &+ \frac{(-1)^{K+2}}{b^{K+2}} \int_0^{\infty} Q^{(K+1)}(\xi) J_{0,K+2}(b\xi) d\xi, \end{aligned} \quad (55)$$

where $J_{0,0}(\xi) \equiv J_0(\xi)$, and $J_{0,\kappa+1}(\xi) = \int_0^\xi J_{0,\kappa}(y)dy + J_{0,\kappa+1}(0)$ with $J_{0,\kappa}(0)$ yet to be defined for $\kappa > 0$. Comparing with (53) gives

$$J_{0,\kappa}(0) = \begin{cases} 1, & \kappa = 0, \\ \frac{(-1)^{(\kappa+1)/2}(\kappa-1)!}{\{2^{(\kappa-1)/2}[(\kappa-1)/2]!\}^2}, & \kappa = 1, 3, 5, \dots, \\ 0, & \kappa = 2, 4, 6, \dots \end{cases}$$

Surprisingly, under this condition

$$\int_0^\infty Q^{(K+1)}(\xi)J_{0,K+2}(b\xi)d\xi = O\left[J_{0,K+2}(0)Q^{(K+1)}(0)\right] \quad (56)$$

not only for rapidly decaying integrands like $Q(\xi) = \xi^n e^{-a\xi^2}$, but even for slower vanishing $Q(\xi) = \xi^n e^{-a\xi}$. Moreover, (56) is correct even for the function $Q(\xi) = (\xi+z)^{-1}$, $z > 0$, which decays for $\xi \rightarrow \infty$ really slowly. These facts can be shown by direct integration and expansion of the result into series of inverse powers of b . They indicate that expansion (55)-(56) of Hankel integrals (48) may have a very general nature similar to expansions (28) for Fourier integrals (25).

>From (46), (54) and because of the relationship

$$\left. \frac{d^{2\kappa}\xi F_j(\xi)}{d\xi^{2\kappa}} \right|_{\xi=0} = 2\kappa F_j^{(2\kappa-1)}(0),$$

we have

$$B_l^{(j,M)} = C_l^{(j)} + 2\pi h^2 \sum_{\kappa=1}^K \frac{(-1)^\kappa 2\kappa(2\kappa)! \Psi_\kappa(l/2M)}{(2^\kappa \kappa!)^2 (4\pi h M)^{2\kappa+1}} F_j^{(2\kappa-1)}(0) \\ + O\left\{ \frac{4h^2 \sqrt{\pi(K+1)} \Psi_{K+1}(l/2M)}{(4\pi h M)^{2K+3}} F_j^{(2K+1)}(0) \right\}, \quad (57)$$

where $-M+1 \leq l_1, l_2 \leq M$, $j = 1, 2$,

$$\Psi_\nu(\alpha) = \sum_{\mu \in \mathbf{Z}^2 \setminus \{0\}} \frac{1}{|\alpha - \mu|^{2\nu+1}}, \quad (58)$$

and the upper bound was used in the error term of the expansion.

3.3 Crucial implementation issues and parallelization

The calculation of high order derivatives of $F_j(\xi)$ for $\xi = 0$ has been considered in Section 2.5. So, the only remaining problem in computing the coefficients $B_l^{(j,M)}$ is the estimation of the series (58). Cutting this series off at $|\mu| = M_\infty$, results in the residual of order $M_\infty^{-2\nu+1}$, which, similar to the one-dimensional case, gives in the worst case $\nu = 1$ the rate

of convergence M_∞^{-1} . Taking into account the two-dimensional nature of (58), this makes it even less realistic to calculate the sum directly.

In order to accelerate the convergence of series (58), we transform it as follows:

$$\begin{aligned} \Psi_\nu(\boldsymbol{\alpha}) = & \sum_{\boldsymbol{\mu} \in \mathbf{Z}^2 \setminus \{0\}} \left(|\boldsymbol{\alpha} - \boldsymbol{\mu}|^{-2\nu-1} - \sum_{\lambda_1=0}^{\Lambda_\nu} \sum_{\lambda_2=0}^{\Lambda_\nu} \frac{\alpha_1^{\lambda_1} \alpha_2^{\lambda_2}}{\lambda_1! \lambda_2!} \frac{\partial^{\lambda_1+\lambda_2} |\boldsymbol{\alpha} - \boldsymbol{\mu}|^{-2\nu-1}}{\partial \alpha_1^{\lambda_1} \partial \alpha_2^{\lambda_2}} \Big|_{\boldsymbol{\alpha}=0} \right) \\ & + \sum_{\lambda_1=0}^{\Lambda_\nu} \sum_{\lambda_2=0}^{\Lambda_\nu} \frac{\alpha_1^{\lambda_1} \alpha_2^{\lambda_2}}{\lambda_1! \lambda_2!} \sum_{\boldsymbol{\mu} \in \mathbf{Z}^2 \setminus \{0\}} \frac{\partial^{\lambda_1+\lambda_2} |\boldsymbol{\alpha} - \boldsymbol{\mu}|^{-2\nu-1}}{\partial \alpha_1^{\lambda_1} \partial \alpha_2^{\lambda_2}} \Big|_{\boldsymbol{\alpha}=0}, \end{aligned} \quad (59)$$

which is actually a kind of Kummer's transformation. The residual of the transformed series

$$\sum_{\boldsymbol{\mu} \in \mathbf{Z}^2 \setminus \{0\}} \left(|\boldsymbol{\alpha} - \boldsymbol{\mu}|^{-2\nu-1} - \sum_{\lambda_1=0}^{\Lambda_\nu} \sum_{\lambda_2=0}^{\Lambda_\nu} \frac{\alpha_1^{\lambda_1} \alpha_2^{\lambda_2}}{\lambda_1! \lambda_2!} \frac{\partial^{\lambda_1+\lambda_2} |\boldsymbol{\alpha} - \boldsymbol{\mu}|^{-2\nu-1}}{\partial \alpha_1^{\lambda_1} \partial \alpha_2^{\lambda_2}} \Big|_{\boldsymbol{\alpha}=0} \right), \quad (60)$$

cut off at $|\boldsymbol{\mu}| = M_\infty$ is of order $M_\infty^{-2\nu-1+\Lambda_\nu}$, and by choosing a proper value of Λ_ν it is easy to obtain the required accuracy of summation for practically acceptable values of M_∞ of order 100.

Transformation (59) reduces the problem of summation of (58) to the calculation of numbers

$$\sum_{\boldsymbol{\mu} \in \mathbf{Z}^2 \setminus \{0\}} \frac{\partial^{\lambda_1+\lambda_2} |\boldsymbol{\alpha} - \boldsymbol{\mu}|^{-2\nu-1}}{\partial \alpha_1^{\lambda_1} \partial \alpha_2^{\lambda_2}} \Big|_{\boldsymbol{\alpha}=0} \quad (61)$$

for a set of integer parameters λ_1 , λ_2 , and ν . For $\nu > 4$ the series (58) converge reasonably fast without any transformations. For $\nu \leq 4$, in order to provide accuracy of summation on the level of machine precision, it is sufficient to take $\Lambda_\nu = 6 - 2(\nu - 1)$.

All practically important cases of (61) can be reduced to the values of the series

$$\psi_{\lambda,\nu}^{(j)} = \sum_{\boldsymbol{\mu} \in \mathbf{Z}^2 \setminus \{0\}} \frac{\mu_j^{2\lambda}}{(\mu_1^2 + \mu_2^2)^{\nu+1/2}}, \quad j = 1, 2, \quad (62)$$

for $1 \leq \nu \leq 7$ and $\max\{\nu - 4, 0\} \leq \lambda \leq \text{int}[(\nu - 1)/2]$. Generally speaking, we would have to consider infinite sums of terms like $\mu_1^{\tilde{\lambda}_1} \mu_2^{\tilde{\lambda}_2} |\boldsymbol{\mu}|^{-2\nu-1}$. However, if at least one of $\tilde{\lambda}_j$, $j = 1, 2$, is odd, then the contribution of the corresponding series both to (60) and (61) will be zero. On the other hand, terms with both even $\tilde{\lambda}_j$ can be reduced to a linear combination of (62). For example, $\mu_1^2 \mu_2^2 |\boldsymbol{\mu}|^{-2\nu-1} = (\mu_1^2 \mu_2^2 + \mu_2^4 - \mu_2^4) |\boldsymbol{\mu}|^{-2\nu-1} = \mu_2^2 |\boldsymbol{\mu}|^{-2\nu+1} - \mu_2^4 |\boldsymbol{\mu}|^{-2\nu-1}$. Obviously, $\psi_{\lambda,\nu}^{(1)} = \psi_{\lambda,\nu}^{(2)}$, which gives immediately

$$\psi_{1,\nu}^{(j)} = \frac{1}{2} \psi_{0,\nu-1}^{(j)} = \frac{1}{2} \sum_{\boldsymbol{\mu} \in \mathbf{Z}^2 \setminus \{0\}} \frac{1}{(\mu_1^2 + \mu_2^2)^{\nu-1/2}}, \quad j = 1, 2. \quad (63)$$

Unfortunately, the symmetry in j does not help so much for $\lambda > 1$.

For $\lambda \geq 0$ the series (62) can be rewritten as follows

$$\psi_{\lambda,\nu}^{(j)} = 2[1 + \text{sign}(\lambda)]\zeta(2\nu - 2\lambda + 1) + 4 \sum_{\mu_1=1}^{\infty} \sum_{\mu_2=1}^{\infty} \frac{\mu_j^{2\lambda}}{(\mu_1^2 + \mu_2^2)^{\nu+1/2}},$$

where the series in the right hand side can be represented by the formula

$$\begin{aligned} \sum_{\mu_1=1}^{\infty} \sum_{\mu_2=1}^{\infty} \frac{\mu_j^{2\lambda}}{(\mu_1^2 + \mu_2^2)^{\nu+1/2}} &= \frac{2^{-2\nu+2\lambda} \sqrt{\pi}}{\Gamma(\nu + 1/2)} \sum_{\kappa_1=0}^{\lambda} c_{\lambda,\kappa_1}(\nu) \left[\frac{\sqrt{\pi} \Gamma(2\nu - 2\lambda) \zeta(2\nu - 2\lambda)}{2^{\kappa_1} \Gamma(\nu - 2\lambda + \kappa_1 + 1/2)} \right. \\ &\quad - \frac{\Gamma(2\nu - 2\lambda + 1) \zeta(2\nu - 2\lambda + 1)}{2^{\kappa_1+1} \Gamma(\nu - 2\lambda + \kappa_1 + 1)} \\ &\quad \left. + \frac{(-1)^{\lambda-\kappa_1}}{2^{\lambda-1}} \sum_{\kappa_2=1}^{\infty} \sum_{\kappa_3=1}^{\infty} \left(\frac{4\pi\kappa_2}{\kappa_3} \right)^{\nu-\lambda} \mathcal{D}_{\nu-\lambda}^{(2\lambda-2\kappa_1)}(2\pi\kappa_2\kappa_3) \right]. \end{aligned} \quad (64)$$

Details of the evaluation of this formula and expressions for $\mathcal{D}_{\nu-\lambda}^{(2\lambda-2\kappa_1)}$ are given in the Appendix 7.2.

Unlike the terms of the double series in the left hand side of (64), terms of the double series in the right decay exponentially and, within the required values of integer parameters ν and λ , accuracy on the level of machine zero $\varepsilon_M \approx 10^{-16}$ is reached for $\kappa_2, \kappa_3 \leq 10$. In practice, a generic work station had calculated all the required numbers (64) in a fraction of a second. The calculations has been carried out in Matlab¹ and results are given in the Appendix too. The algorithm was validated by comparison with the direct summation for large enough values of ν and with formula (63).

The coefficients $C_l^{(j)}$ from (57) have been calculated by direct numerical integration. Similarly to the one-dimensional case, the integrands in (43), (44) are very smooth and fast decaying functions which makes integration very efficient. The only difference is that the integration should be done on the sequence of intervals between zeros of $J_0(2\pi h l \xi)$, see e.g. [1], rather than between zeros of $\cos(2\pi h l \xi)$. An attempt to accelerate the convergence by the ε -algorithm halved processing time, on average, however failed to produce reliable estimation of the accuracy. Thus, if accuracy is of primary interest, then it is safer to carry out the integration straightforwardly.

The convolution coefficients (57) are point-wise and the parallelization of their calculations represents no problems. On average, in our practice, these calculations take about the same amount of computer resources as a few dozens of time steps. In contrast, at least a few dozens of thousands of time steps is usually required in order to obtain the numerical solution to (1) on a physically meaningful time scale.

In parallel implementation, the coordinate direction-wise nature of the time marching algorithm suggests to split the core data of $4M \times 4M$ elements between P processors in the form of P arrays of $4M \times (4M/P)$ elements. The repeating alteration of processing between x_1 and x_2 directions prompts to keep a copy of the data split between processors along another direction into P arrays of $(4M/P) \times 4M$ elements as well (see Fig. 9). In both copies of the data the longest direction corresponds to the first index of the array

¹Standard Fortran routines for K_ν available in NETLIB were found not accurate enough to compete with Matlab

in order to enhance the use of cash memory. Before switching the direction of processing, alternative arrays of data are upgraded by using `MPI_GATHERV` routine. Optimal load balancing is reached by setting P as a factor of $4M$.

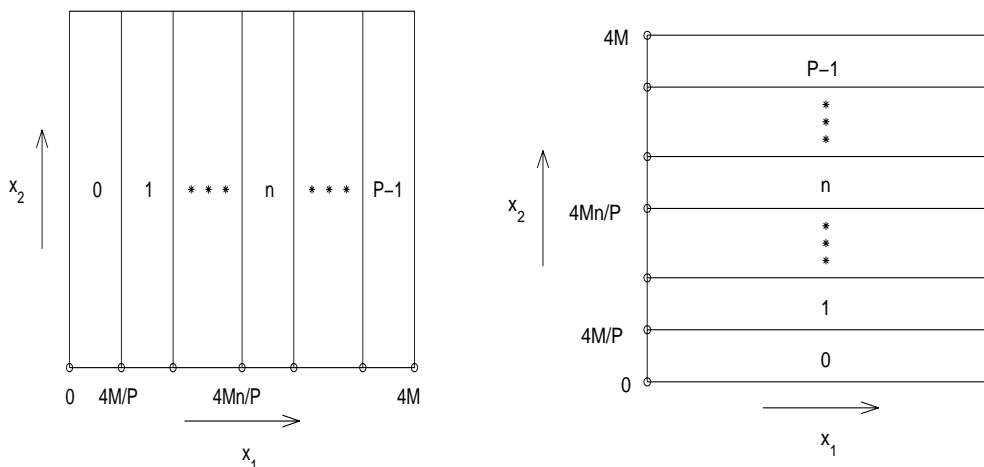


Figure 9: Two copies of data distributed among P processors in x_2 and x_1 directions.

Computational codes were written in Fortran 90 and in the two dimensional case MPI has been chosen as the parallelization tool. The chosen data structure allows efficient use of the standard sequential routines for the discrete Fourier transform in (47) and LU-sweeps in (37). Standard routines from both NETLIB [17] and NAG [16] have been tested. FFT routines from NETLIB's FISHPACK have appeared to be as efficient and accurate as those from the NAG. However, numerical quadrature D01AKE from NAG Fortran Library looked more attractive (at least more accurate) than its QUADPACK's counterpart DQAGS.

The MPI code was validated by comparison against the results obtained with the sequential code for a relatively small computational domain with $L = 10\pi$. The discrepancy was on a level of 3-4 decimal digits less than machine precision, which is in a good agreement with the accuracy of the quadrature routines used by the parallel code (D01AKE). The sequential code was run on Origin 200 and the parallel one on CRAY T3E-1200.

Dependence of the acceleration gained from multiprocessing in regards to the use of a single processor is depicted in Fig. 10. The measurements have been taken by running the code for a fixed number of time steps. For 128 processors the graph reveals efficient level of parallelization at about 23%. In these runs main data arrays were of 512×512 elements.

It looks like that the main contribution into deviation from the theoretical predictions of parallel performance comes from the `MPI_GATHERV` procedure which is used repeatedly during every time step in order to transform data arrays from x_1 to x_2 orientation and vice verse (see Fig. 9).

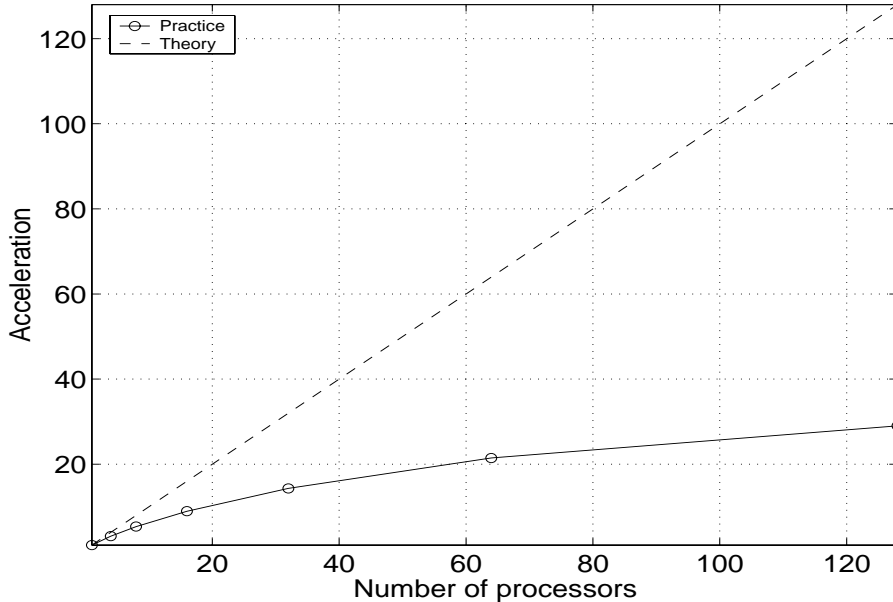


Figure 10: Parallel performance of the code on CRAY T3E-1200.

4 Results of numerical experiments

4.1 Accuracy

The accuracy of the algorithm was tested on steady coalescent pole solutions (4), (5) in relatively small domains $L < L_c$. For $N_p = 1$, steady-state solution corresponds to $b_1 = (L/4\pi) \ln[(\gamma L + 4\pi)/(\gamma L - 4\pi)]$. For $N_p > 1$ the values of b_1, \dots, b_{N_p} , have been calculated by Newton iterations as steady-state solutions to (5).

In practice, for numerical grids with $0.001 < h < 0.1$, the theoretical order of approximation was reached for up to the fourth order of approximation. For algorithms of higher orders real approximation was not better than of the fifth order. Therefore, from the point of view of computational efficiency, it is expedient to use the algorithm of at most of the sixth order or even of the fourth one for this range of h . In our practice, by proper choice of D , h , and of the order of approximation, it was always possible to obtain the relative residual of the approximation of (2) on the steady coalescent pole solutions up to 10^{-10} .

Limitations of the accuracy of the algorithm come from variety of reasons. In particular, from errors of the numerical integration to compute the convolution coefficients (17) and (18) in (30). Further, high order derivatives of steady coalescent N_p -pole solutions grow very fast with their order. Hence, the high formal order of the approximation might only be observed for smaller values of h than those used in this work.

It was possible to reach the relative accuracy of approximation of the stabilized solution to (2) in comparison to $\Phi_{N_p, L}(x, t)$ of order 10^{-10} for $\gamma L < 12\pi$ (i.e. for $N_{p, L} = 1$) as well. However, this accuracy of the approximation of $\Phi_{N_p, L}(x, t)$ by the steady state of (2) was rapidly degrading with L growing. This degradation of the accuracy of the stabilized numerical solution is in agreement with the high sensitivity of the steady coalescent pole solutions to noise. Taking into account results of [6], some of the constants C_i , $i = 1, 2, 3$

in the a priori estimation

$$\|\Phi_{N_p,L}(x,t) - \lim_{t \rightarrow \infty} \Phi_h(x,t)\|_2 \leq C_1 h^N + C_2 \varepsilon(D) + C_3 \varepsilon_M \quad (65)$$

might be of order of $e^{O(L)}$. Assuming that the round-off errors are pseudorandom, it is most likely that C_3 is of order of $e^{O(L)}$. However, other constants can be much less because the transient amplification usually occurs for perturbations of very special type only, to which the deterministic approximation residuals may not belong if $\Phi \approx \Phi_{N_p,L}$.

The last issue relevant to the accuracy, which we would like to mention here, is the Φ - and x -shift invariance of the Sivashinsky equation. In other words, it means that if $\Phi(x,t)$ is a solution, then, for any real $\Delta\Phi$ and Δx , the function $\Phi(x + \Delta x, t) + \Delta\Phi$ satisfies the Sivashinsky equation as well. Thus, the shifts of the stabilized solution are not known a priori and should be identified in order to allow comparison with the exact solution. The only way to estimate the shifts is by a kind of optimization. In particular, calculation of the minimum of the stabilized solution was carried out in this work. Generally speaking, errors of the estimation of the minimum might interfere or even supersede the errors made during the calculation of the solution itself.

It can be checked by direct substitution that if $\Phi^{(1)}(x,t)$ and $\Phi^{(2)}(x,t)$ are solutions to one-dimensional equation (2), then the function

$$\Phi(x_1, x_2, t) = \Phi^{(1)}(x_1, t) + \Phi^{(2)}(x_2, t) \quad (66)$$

is a solution to the two dimensional equation (1). In our numerical experiments the functions

$$\Phi_{N_p,L}(x_1, x_2, t) = \Phi_{N_p,L}(x_1, t) + \Phi_{N_p,L}(x_2, t) \quad (67)$$

were found to be the steady attractors for Sivashinsky's equation in two dimensions for small enough L . These solutions were used in order to test the accuracy of the algorithm in two space dimensions.

The parameters of the two-dimensional algorithm have a similar qualitative effect on its accuracy as in the one-dimensional case. However, quantitatively, the accuracy of the algorithm in two-dimensions is usually less by one or two decimal digits for the same sets of parameters. Also, understandably, the choice of two-dimensional grids with small values of h is more restrictive in practice.

4.2 One-dimensional equation

The typical evolution of the flame front in a relatively small domain $L = 50\pi < L_c$ is shown in Fig. 11. In the very beginning the flame rapidly approaches a steady coalescent N_{p,L_0} -pole solution with the period $L_0 = 10\pi$ of the initial condition. Later, the solution undergoes a series of bifurcations and stabilizes to the steady coalescent $N_{p,L}$ -pole solution with the period L occupying the entire computational domain.

Appearance and disappearance of poles in $\Phi(x,t)$ can be clearly seen in the graph of its spatially averaged time derivative:

$$\langle \Phi_t \rangle = L^{-1} \int_{-L/2}^{L/2} \frac{\partial \Phi}{\partial t} dx. \quad (68)$$

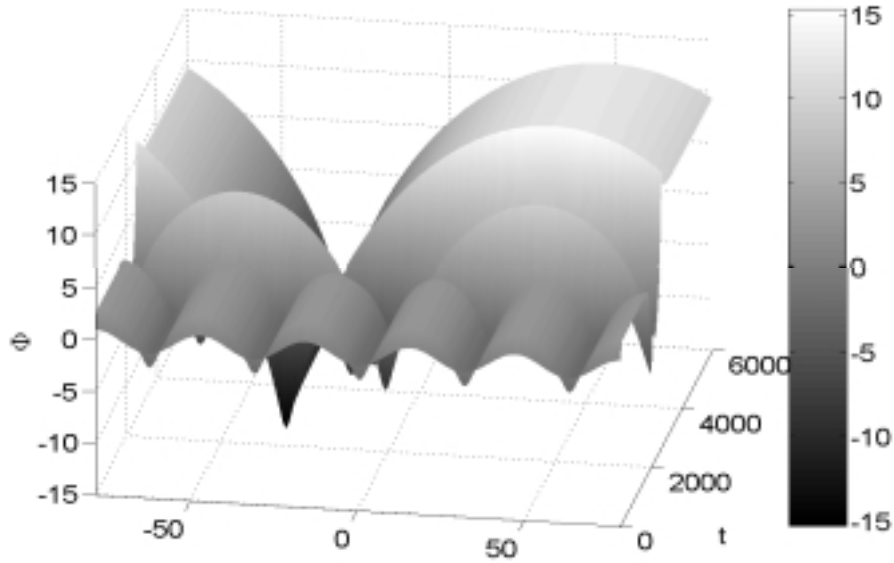


Figure 11: Evolution of the flame front profile in time for $L = 50\pi$, $\gamma = 0.8$, and $\Phi(x, 0) = -\cos 10\pi x/L$.

Physically, $\langle \Phi_t \rangle$ is the increase of the speed of the flame front in comparison with the speed of the plane laminar flame. For steady coalescent N_p -pole solution (4) we obviously have

$$\langle \Phi_t \rangle = 2\pi N_p L^{-1} (\gamma - 4\pi N_p L^{-1}). \quad (69)$$

The behaviour of $\langle \Phi_t \rangle$ for time-dependent solutions to (2) is essentially different. In moments of time which, in terms of (4), correspond to a change in the number of poles per period, function (68) develops sharp spikes, see Fig. 12. The Figure shows also that with time all such spikes die out eventually, indicating stabilization of the solution to $\Phi_{N_p, L}(x)$ for any initial conditions. The function $\langle \Phi_t \rangle$ does not develop sharp spikes for time-dependent pole solutions (4) because the number of poles in (5) is the integral of the system.

Scenario changes dramatically when the length of the computational domain exceeds a critical value L_c . In this case, sharp spikes in $\langle \Phi_t \rangle$ do not die out but appear and appear for as long as computations are continued. For some initial conditions transition to the essentially time-dependent asymptotic for $t \rightarrow \infty$ can be quite delayed, as it is illustrated in Fig. 13 for $L = 100\pi$. Close examination of solutions to (2) shows that the appearance of spikes coincides with the appearance of micro cusps on the surface of the flame front as illustrated in Fig. 2. In terms of pole solutions (4) these micro cusps would correspond to additional poles appearing near the crest of the flame profile, then moving slowly towards its trough, and eventually disappearing there.

The problem of finding the value of L_c by direct numerical simulations is rather time consuming. Figures 14 and 15 illustrate, for example, the behaviour of $\langle \Phi_t \rangle$ for $L \approx L_c$. It seems, on the first look, that $\langle \Phi_t \rangle$ has stabilized and $\gamma L_c > 68\pi$. However, after waiting some time, chaotic oscillations eventually appear on a really small scale. Hence, γL_c is slightly less than 68π and after a few more runs we have concluded that in this particular case $\gamma L_c \approx 68\pi$. The importance of the parameter $\langle \Phi_t \rangle$ can be seen from Fig. 14 showing

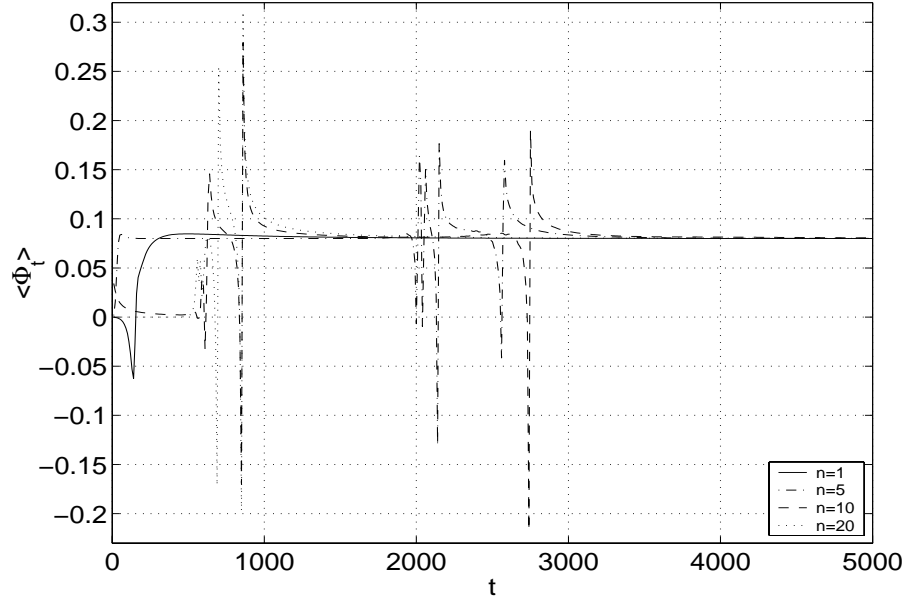


Figure 12: Dependence of $\langle \Phi_t \rangle$ on time for $L = 50\pi$, $\gamma = 0.8$, and $\Phi(x, 0) = -\cos 2\pi n x / L$.

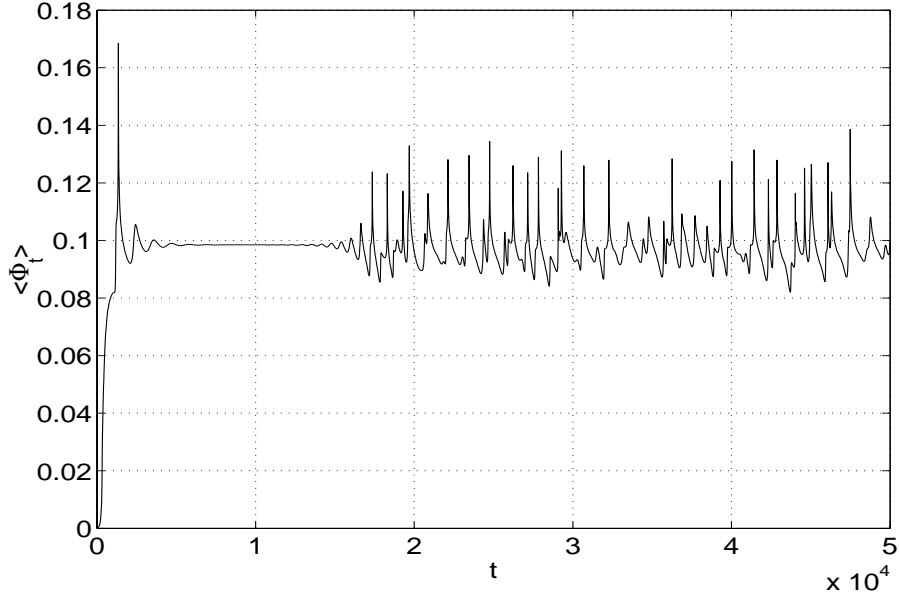


Figure 13: Dependence of $\langle \Phi_t \rangle$ on time for $L = 100\pi$, $\gamma = 0.8$, and $\Phi(x, 0) = -\cos 2\pi x / L$.

clearly and in a relatively short time that the “stabilized” value of $\langle \Phi_t \rangle$ is about 0.09, which exceeds the theoretical value of 0.08 for corresponding steady coalescent $N_{p,L}$ -pole solution. Two values of L_c obtained in our calculations with 32- and 64-bit arithmetics are shown in Fig. 16. Accuracy of observations was at least $\pm 4\pi$. Note, that corresponding machine zeros were $\varepsilon_M \approx 10^{-7}$ and 10^{-16} , and in calculations with 32-bit arithmetics round-off errors clearly dominated discretization errors.

An analytical attempt to estimate the value of L_c was made in [6] where the following

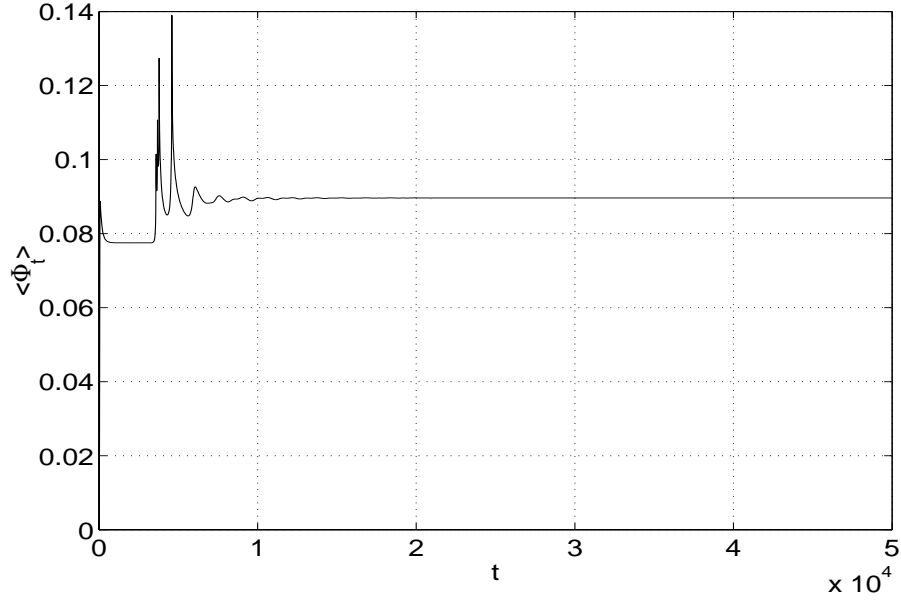


Figure 14: Dependence of $\langle \Phi_t \rangle$ on time for $L = 85\pi$, $\gamma = 0.8$, and $\Phi(x, 0) = -\cos 10\pi x/L$.

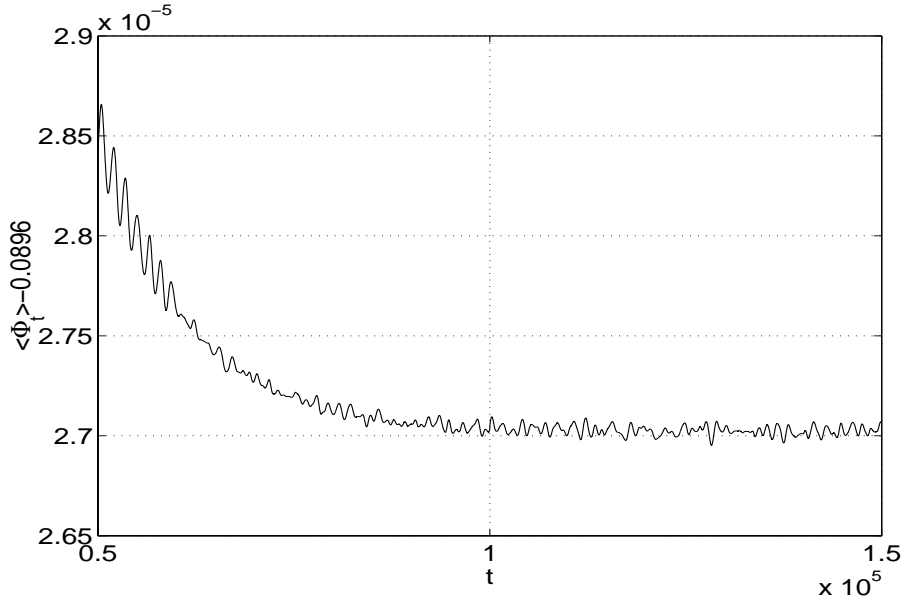


Figure 15: Dependence of $\langle \Phi_t \rangle$ on time for $L = 85\pi$, $\gamma = 0.8$, and $\Phi(x, 0) = -\cos 10\pi x/L$; continuation of Fig. 14.

modification of (2) linearized on the steady coalescent pole solution was considered:

$$\frac{\partial \Delta \Phi}{\partial t} - x R^{-1} \frac{\partial \Delta \Phi}{\partial x} = \frac{\partial^2 \Delta \Phi}{\partial x^2} + \frac{\gamma}{2} \frac{\partial \mathcal{H}[\Delta \Phi]}{\partial x}, \quad x \in \mathbf{R}. \quad (70)$$

Here $\Delta \Phi(x, t) = \Phi(x, t) - \Phi_{N_p, L}(x, t)$ and R is the curvature radius in the crest of the flame profile $\Phi_{N_p, L}(x, t)$. The investigation of a particular asymptotic solution to (70) resulted in an estimation of the possible amplification of the spectral density f of harmonics of

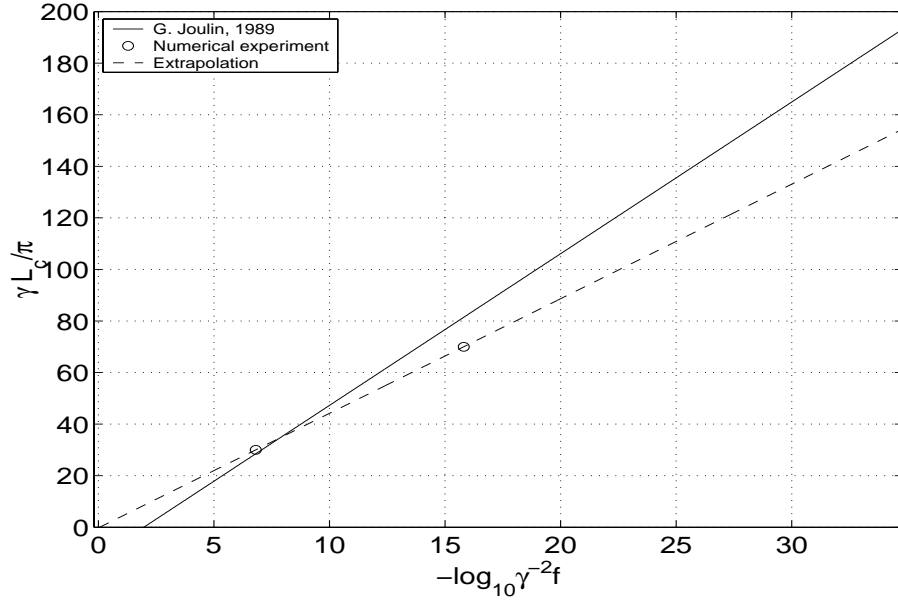


Figure 16: Dependence of the critical period L_c versus the amplitude of the perturbation f .

$\Delta\Phi(x, 0)$ versus R . The latter provides values of the critical curvature radius R_c for which the spectral density of the most dangerous harmonics can grow up to the order of $O(1)$. A functional link between L and R can be easily established for $\Phi_{N_p, L}(x, t)$ and the resulting graph of L_c versus f is shown in Fig. 16.

The agreement is striking because results in [6] have been obtained for the spectral density of the most dangerous harmonic of the perturbation $\Delta\Phi(x, 0)$ rather than for its amplitude resulting in overestimation of L_c . Also, the value of L_c in [6] corresponds to amplification of the most dangerous harmonic up to the order of $O(1)$, while in our computational practice we were judging L_c by its “stabilized” value of $\langle\Phi_t\rangle$ which results in underestimation of L_c . The use of normalizing parameters κ_1 and κ_2 such that $\kappa_1 f$ and $\kappa_2 O(1)$ replace f and $O(1)$ correspondingly gives exact coincidence of graphs in Fig. 16 for $\kappa_1 \approx 0.81$ and $\kappa_2 \approx 1.32$.

Effect of the round-off errors in numerical solution of (2) can be modelled by a stochastic right hand side $f(x, t)$ as follows:

$$\frac{\partial\Phi}{\partial t} - \frac{1}{2} \left(\frac{\partial\Phi}{\partial x} \right)^2 = \frac{\partial^2\Phi}{\partial x^2} + \frac{\gamma}{2} \frac{\partial\mathcal{H}[\Phi]}{\partial x} + f(x, t), \quad x \in \mathbf{R}. \quad (71)$$

Such an explicit addition to the Sivashinsky equation was studied, for example, in [3], [2], [4], and [18]. Solutions to (71) are no longer similar under the condition $\gamma L = const$. In order to preserve similarity (3) for (71), one needs to impose the condition $\gamma_1^{-2} f_1 = \gamma_2^{-2} f_2$ alongside with $\gamma_1 L_1 = \gamma_2 L_2$. Otherwise, if $|f|$ is fixed, the single relationship $\gamma L_c = const$ is no longer the condition of invariance and both values of L and γ are of importance. In particular, it should be specified that the calculations for Fig. 16 have been carried out for $\gamma = 0.8$. This correction is not essential if the considered values of γ are of order 1 because of the logarithmic dependence between L_c and $|f|$. However, generally speaking, the additional condition of the invariance for the nonuniform equation (71) may have

important implications for the interpretation of results of simulations.

Unlike (2) has been obtained under the assumption of small heat expansion $\gamma \ll 1$, it can be considered for any value of $\gamma > 0$ and, then, interpreted for a physically acceptable value of γ' but in a larger domain L' in virtue of the invariance condition $\gamma L = \gamma' L'$. With addition of the noise term in (71) we have to request also, that the noise level in a realistic system with small heat expansion is proportionally smaller $f' = (\gamma')^2 \gamma^{-2} f$. The effect of physical noise in the derivation of Sivashinsky's equation (1) was not addressed properly yet, and it maybe different of what is imposed by the additive structure of (71). Thus, the additive inclusion of the noise into the Sivashinsky equation models the effect of round-off errors in numerical experiments with this equation quite good, but it maybe wrong from physical point of view.

4.3 Two-dimensional equation

Qualitatively, the temporal behaviour of the two-dimensional flame fronts is similar to the one-dimensional one. Figures 17 and 18 illustrate the evolution of a relatively small flame in two spatial dimensions. Unlike starting from initial condition $\Phi(\mathbf{x}, 0) = -\cos(10\pi x_1/L) \cos(10\pi x_2/L)$, which is not additive in coordinate directions, the solution is rapidly transformed into the additive form (66) and is very close to $\Phi_{1,10\pi}(x_1, t) + \Phi_{1,10\pi}(x_2, t)$ for some time. Later, the first summand begins to evolve and for $t \approx 1050$ the solution is approximately equal to $\Phi_{N_L, L}(x_1, t) + \Phi_{1,10\pi}(x_2, t)$. Only then the second summand begins to bifurcate and the flame front reaches eventually the steady shape composed of the sum of two one-dimensional steady coalescent $N_{p, L}$ -pole solutions (67).

Similar scenarios were observed in our simulations with a variety of other initial conditions and values of L . In all the cases the period of the intermediate flame shapes of the additive form (66) was determined by the period of the initial condition if the latter was greater than the neutral wavelength $4\pi/\gamma$ of the dispersion relationship associated with (1). For initial conditions with smaller wavelengths the intermediate shape was just close to zero.

The nonstationary asymptotic character of solutions to the two-dimensional Sivashinsky equation for larger L is illustrated in Fig. 19 in the form of the dependence of the spatially averaged speed of the flame front on time. Here, the perturbations, appearing on the flame surface randomly in time, look like cracks aligned parallel to the x_1 -axis and moving along the x_2 -coordinate. The $x_1 = \text{const}$ cross-sections of the cracks are very similar to the micro cusps observed in one spatial dimension. The cracks lined up parallel to the x_2 -axis were not observed in our calculations for L up to 90π . This is, probably, because of the asymmetrical treatment of the spatial coordinate directions implemented in the computational algorithm.

It was found out in our calculations with 64-bit arithmetic, that for the two independent spatial dimensions the value of γL_c is likely to be slightly less than 68π , but does not differ from it significantly. In hydrodynamics, reduction of the critical Reynolds number with the increase of the dimension of the problem is a distinctive characteristic of the nonmodal instability, see [26].

The two-dimensional Sivashinsky equation (1) was not as popular among researchers as its one-dimensional counterpart (2). The paper [15] is one of a few, if not the only one, where (1) was studied numerically. Similar to the one-dimensional case, there is a very

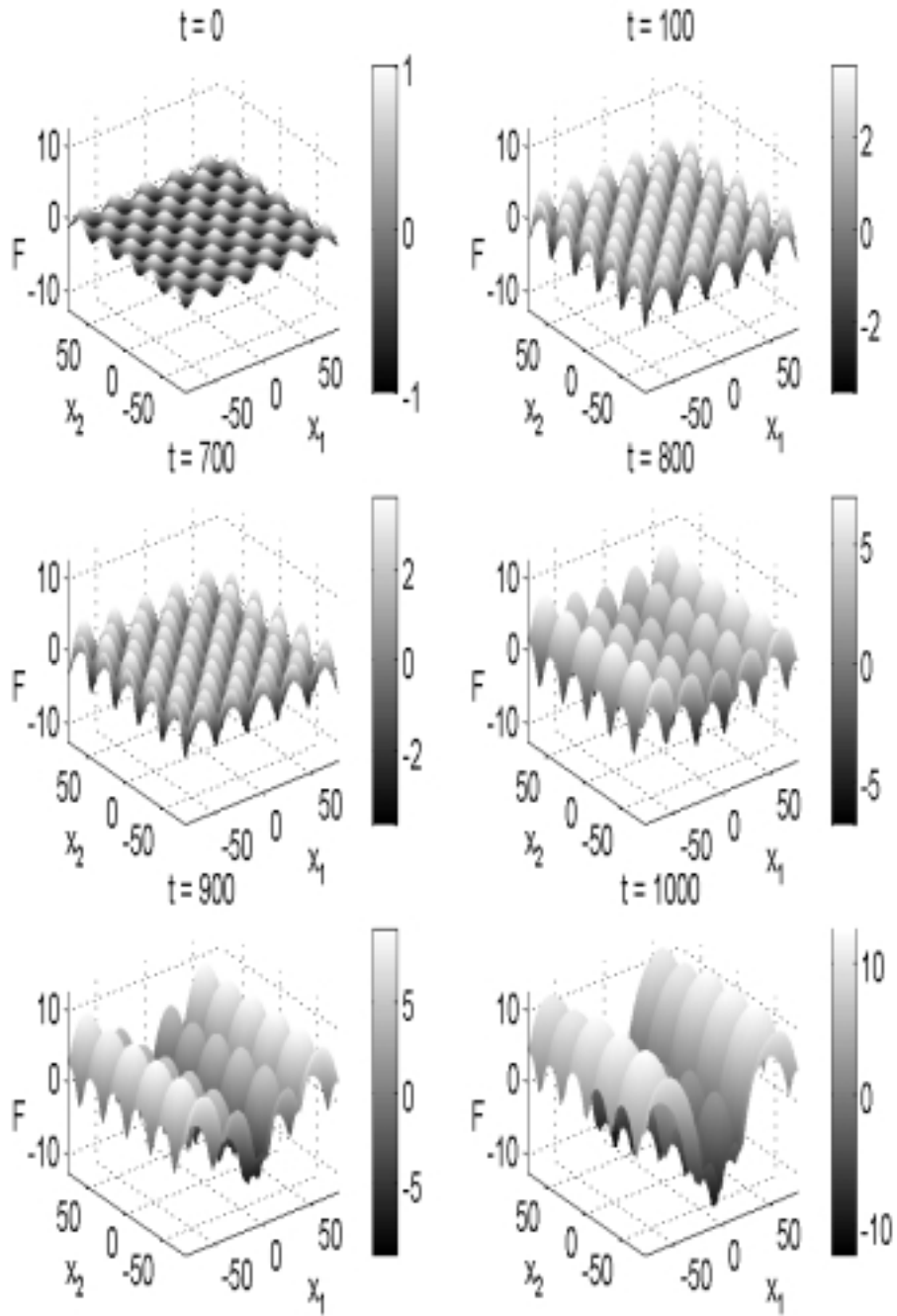


Figure 17: Evolution of the flame front profile in time for $L = 50\pi$, $\gamma = 0.8$, and $\Phi(x_1, x_2, 0) = -\cos(10\pi x_1/L) \cos(10\pi x_2/L)$.

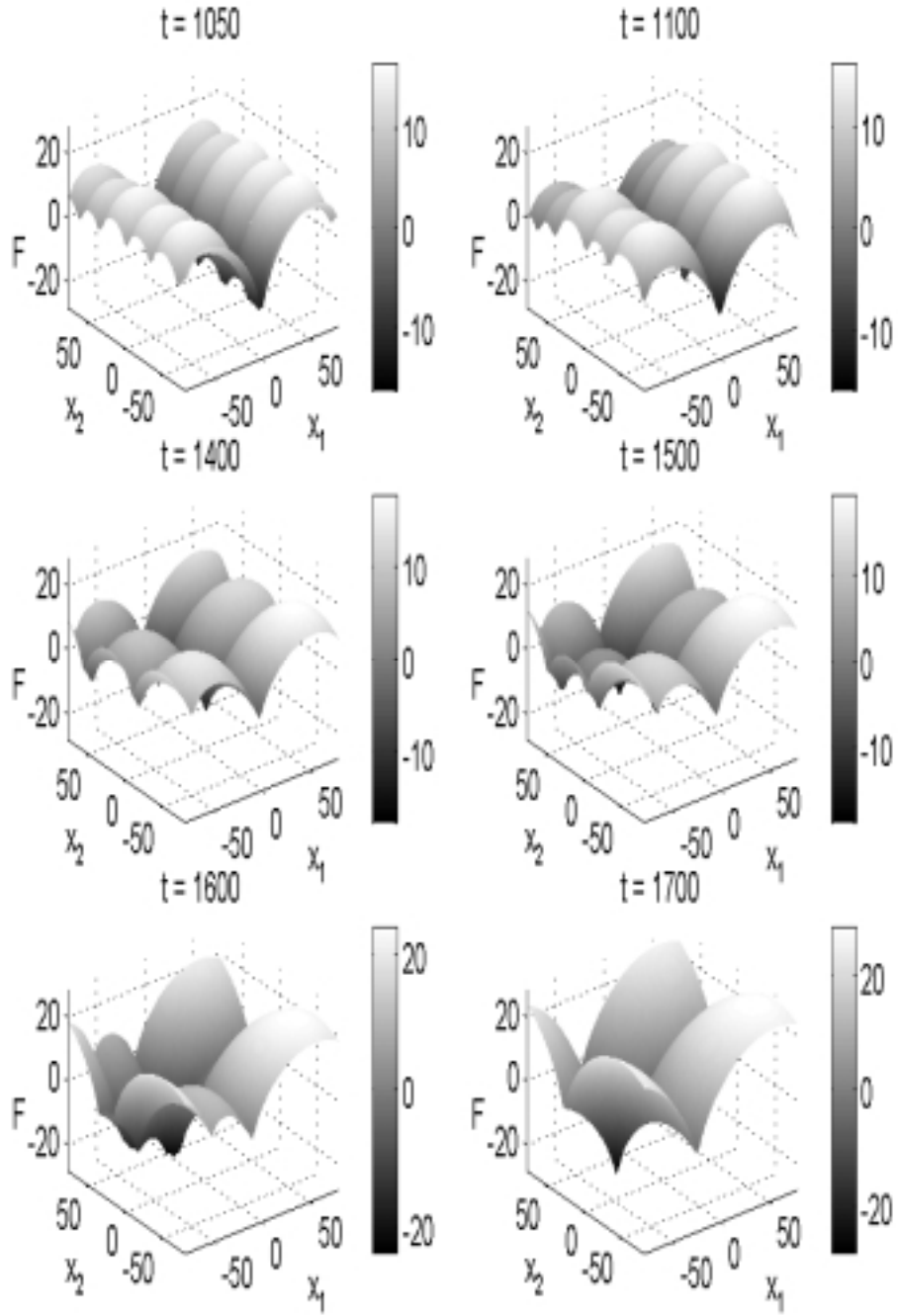


Figure 18: Evolution of the flame front profile in time for $L = 50\pi$, $\gamma = 0.8$, and $\Phi(x_1, x_2, 0) = -\cos(10\pi x_1/L) \cos(10\pi x_2/L)$; continuation of Fig. 17.

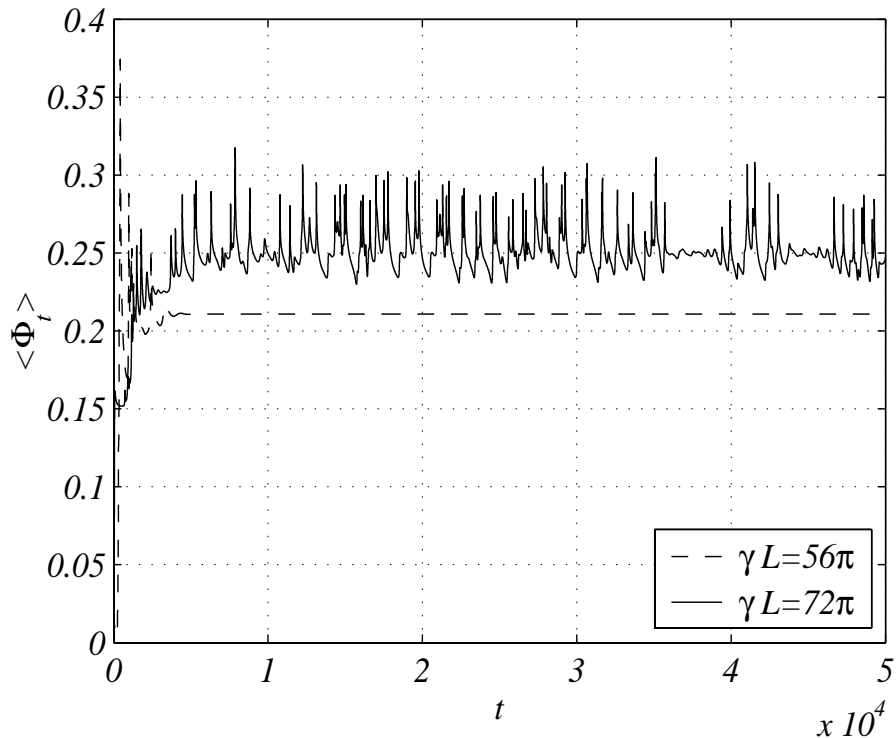


Figure 19: Dependence of $\langle \Phi_t \rangle$ on time in the two-dimensional case for $L = 70\pi$ and $L = 90\pi$. Here $\gamma = 0.8$ and $\Phi(x_1, x_2, 0) = -\cos(n\pi x_1/L) \cos(n\pi x_2/L)$ with $n = 20$ and 10 for $L = 70\pi$ and 90π correspondingly.

good agreement between our results and data from [15], where a spectral method was used.

5 Conclusions

Efficient and high accurate computational algorithms for periodic solutions to the Sivashinsky equation in one and two spatial dimensions have been proposed. The algorithms are based on "approximate approximations". Generally speaking, the accuracy of the method of "approximate approximations" is only limited by the smoothness of approximated solutions. On the other hand, the accuracy of the "approximate approximation" is only degraded locally if the smoothness of the approximated function is lost locally. The latter property of the method proved to be useful for bifurcating solutions with smoothness degrading in moments of bifurcations.

Results of the implementation of our computational code on CRAY T3E-1200 have shown reasonable parallel efficiency of the approach. Resources for improving the performance of the code and of the overall efficiency of the numerical approach and computational algorithm have been discussed as well.

Unlike the presentation of the algorithms through its application to the Sivashinsky equation, it can be straightforwardly applied to a wide class of nonlinear nonlocal pseudodifferential equations.

The given examples of computations not only demonstrate the accuracy and efficiency of the algorithms but, also, confirm at a reasonable level of confidence that flame fronts governed by Sivashinsky's equation become extremely sensitive to external perturbations as their size grows. This sensitivity was not caused by the special structure of the limiting solutions, formed by a set of coalescent poles, but it is a consequence of the nonnormality of the linearized governing operator. A similar effect was also discovered in many other systems, for example in Hagen-Poiseuille flow, where pole solutions have not been found.

6 Acknowledgements

This research was supported by the EPSRC grants GR/K95932 and GR/R66692 and by the computer resources grant cs2014.

7 Appendix

7.1 Estimation of the accuracy of the expansion (30)

In order to make the estimation, we have noticed that

$$\left| \sum_{\mu \in \mathbf{Z} \setminus \{0\}} \left(\mu - \frac{l}{2M} \right)^{-2K_j-2} \right| \leq 2 \sum_{\mu=1}^{\infty} \left(\mu - \frac{|l|}{2M} \right)^{-2K_j-2},$$

because $\mu - \frac{|l|}{2M} \leq \mu + \frac{|l|}{2M}$ for $|l| \leq M$. By taking into account that only values of $|l| \leq M$ are involved into consideration, we have

$$\begin{aligned} \left| \sum_{\mu \in \mathbf{Z} \setminus \{0\}} \left(\mu - \frac{l}{2M} \right)^{-2K_j-2} \right| &\leq 2 \sum_{\mu=1}^{\infty} \left(\mu - \frac{1}{2} \right)^{-2K_j-2} \\ &= 2 \sum_{\mu=0}^{\infty} \left(\mu + \frac{1}{2} \right)^{-2K_j-2} = 2 \frac{\psi(2K_j+1)(1/2)}{(2K_j+1)!}. \end{aligned} \quad (72)$$

The value of $\psi^{(\kappa)}(x)$ for $x = 1/2$ can be expressed in terms of Riemann's zeta function as follows

$$\psi^{(\kappa)}(1/2) = (-1)^{\kappa+1} \kappa! (2^{\kappa+1} - 1) \zeta(\kappa + 1) \quad (73)$$

(see entry 6.4.4, p. 260 of [1]). For $\zeta(2\kappa)$ we have (see entries 23.1.2, p. 804 and 23.1.18, p. 805 of [1]) in turn

$$\zeta(2\kappa) = (-1)^{\kappa-1} \frac{(2\pi)^{2\kappa}}{2(2\kappa)!} B_{2\kappa}, \quad (74)$$

and inequality 23.1.15, p. 805 of [1] yields for Bernoulli number $B_{2\kappa}$

$$|B_{2\kappa}| < \frac{2(2\kappa)!}{(2\pi)^{2\kappa}(1 - 2^{1-2\kappa})}. \quad (75)$$

Gathering (73)-(75), we obtain

$$\psi^{(2K_j+1)}(1/2) < (2K_j + 1)! \frac{(2^{2K_j+2} - 1)}{(1 - 2^{-2K_j-1})} \leq 3(2K_j + 1)! 2^{2K_j+1}. \quad (76)$$

Back to (72) this means:

$$\left| \sum_{\mu \in \mathcal{Z} \setminus \{0\}} \left(\mu - \frac{l}{2M} \right)^{-2K_j-2} \right| \leq 3 \cdot 2^{2K_j+2},$$

and, eventually, (30).

7.2 Calculation of values of the series $\sum_{\mu_1=1}^{\infty} \sum_{\mu_2=1}^{\infty} \mu_j^{2\lambda} |\boldsymbol{\mu}|^{-2\nu-1}$

Applying entry 2.12.8.17, p. 186 of [20], we have

$$\sum_{\mu_1=1}^{\infty} \sum_{\mu_2=1}^{\infty} \frac{\mu_j^{2\lambda}}{(\mu_1^2 + \mu_2^2)^{\nu+1/2}} = \frac{\sqrt{\pi}}{2^\nu \Gamma(\nu + 1/2)} \int_0^\infty \left[\sum_{\mu_j=1}^{\infty} \mu_j^{-\nu+2\lambda} J_\nu(\mu_j x) \right] \frac{x^\nu dx}{e^x - 1}. \quad (77)$$

By using the recurrent relationship $J_\nu(\mu_j x) = 2(\nu - 1)(\mu_j x)^{-1} J_{\nu-1}(\mu_j x) - J_{\nu-2}(\mu_j x)$ (see entry 9.1.27, p. 361 of [1]) repeatedly, the series under the integral in (77) can be written in the form

$$\sum_{\mu_j=1}^{\infty} \mu_j^{-\nu+2\lambda} J_\nu(\mu_j x) = \sum_{\kappa_1=0}^{\lambda} \frac{c_{\lambda, \kappa_1}(\nu)}{x^{\kappa_1}} \sum_{\mu_j=1}^{\infty} \mu_j^{-\nu+2\lambda-\kappa_1} J_{\nu-2\lambda+\kappa_1}(\mu_j x), \quad (78)$$

with coefficients $c_{\lambda, \kappa_1}(\nu)$ given by formulas

$$c_{0,0} = 1,$$

$$c_{1,0} = -1, \quad c_{1,1} = 2(\nu - 1),$$

$$c_{2,0} = 1, \quad c_{2,1} = -4(\nu - 2), \quad c_{2,2} = 4(\nu - 1)(\nu - 2),$$

$$c_{3,0} = -1, \quad c_{3,1} = 6(\nu - 3), \quad c_{3,2} = -12(\nu - 2)(\nu - 3), \quad c_{3,3} = 8(\nu - 1)(\nu - 2)(\nu - 3).$$

The latter transformation provides a chance to use entry 5.7.19.11, p. 678 of [20] which can be written as

$$\begin{aligned} & \sum_{\mu_j=1}^{\infty} \mu_j^{-\nu+2\lambda-\kappa_1} J_{\nu-2\lambda+\kappa_1}(\mu_j x) \\ &= \frac{\sqrt{\pi} x^{\nu-2\lambda+\kappa_1-1}}{2^{\nu-2\lambda+\kappa_1} \Gamma(\nu - 2\lambda + \kappa_1 + 1/2)} - \frac{x^{\nu-2\lambda+\kappa_1}}{2^{\nu-2\lambda+\kappa_1+1} \Gamma(\nu - 2\lambda + \kappa_1 + 1)} \\ &+ \frac{\sqrt{\pi} x^{-\nu+2\lambda-\kappa_1}}{2^{\nu-2\lambda+\kappa_1-1} \Gamma(\nu - 2\lambda + \kappa_1 + 1/2)} \sum_{\kappa_2=1}^{\text{int}(x/2\pi)} (x^2 - 4\pi^2 \kappa_2^2)^{\nu-2\lambda+\kappa_1-1/2}. \end{aligned}$$

Substitution of the last formula and (78) into (77) results in

$$\begin{aligned} \sum_{\mu_1=1}^{\infty} \sum_{\mu_2=1}^{\infty} \frac{\mu_j^{2\lambda}}{(\mu_1^2 + \mu_2^2)^{\nu+1/2}} &= \frac{\pi}{\Gamma(\nu + 1/2)} \sum_{\kappa_1=0}^{\lambda} \frac{2^{-2\nu+2\lambda-\kappa_1} c_{\lambda,\kappa_1}(\nu)}{\Gamma(\nu - 2\lambda + \kappa_1 + 1/2)} \left[\int_0^{\infty} \frac{x^{2\nu-2\lambda-1} dx}{e^x - 1} \right. \\ &\quad - \frac{\Gamma(\nu - 2\lambda + \kappa_1 + 1/2)}{2\sqrt{\pi}\Gamma(\nu - 2\lambda + \kappa_1 + 1)} \int_0^{\infty} \frac{x^{2\nu-2\lambda} dx}{e^x - 1} \\ &\quad \left. + 2 \sum_{\kappa_2=1}^{\infty} \int_{2\pi\kappa_2}^{\infty} \frac{x^{2\lambda-2\kappa_1} (x^2 - 4\pi^2\kappa_2^2)^{\nu-2\lambda+\kappa_1-1/2} dx}{e^x - 1} \right], \end{aligned} \quad (79)$$

where the first two integrals are available from entry 2.3.14.6, p. 341 of [19]. The third one can be expanded into the series

$$\begin{aligned} &\int_{2\pi\kappa_2}^{\infty} \frac{x^{2\lambda-2\kappa_1} (x^2 - 4\pi^2\kappa_2^2)^{\nu-2\lambda+\kappa_1-1/2} dx}{e^x - 1} \\ &= \sum_{\kappa_3=1}^{\infty} \int_{2\pi\kappa_2}^{\infty} x^{2\lambda-2\kappa_1} (x^2 - 4\pi^2\kappa_2^2)^{\nu-2\lambda+\kappa_1-1/2} e^{-\kappa_3 x} dx \\ &= \sum_{\kappa_3=1}^{\infty} \frac{\partial^{2\lambda-2\kappa_1}}{\partial \kappa_3^{2\lambda-2\kappa_1}} \int_{2\pi\kappa_2}^{\infty} (x^2 - 4\pi^2\kappa_2^2)^{\nu-2\lambda+\kappa_1-1/2} e^{-\kappa_3 x} dx, \end{aligned} \quad (80)$$

because every term of this series is analytic in κ_3 . Eventually, the remaining integral is given in entry 2.3.5.4, p. 323 of [19] in terms of the modified Bessel functions $K_{\nu-2\lambda+\kappa_1}(2\pi\kappa_2\kappa_3)$ which decay exponentially for $2\pi\kappa_2\kappa_3 \rightarrow \infty$. Summarizing, (79) can be written as in (64). Expressions for $\mathcal{D}_{\nu-\lambda}^{(2\lambda-2\kappa_1)}(2\pi\kappa_2\kappa_3)$ denoting normalized derivatives from (80) are given below:

$$\begin{aligned} \mathcal{D}_{\nu-\lambda}^{(0)}(2\pi\kappa_2\kappa_3) &= K_{\nu-\lambda}(2\pi\kappa_2\kappa_3), \\ \mathcal{D}_{\nu-\lambda}^{(2)}(2\pi\kappa_2\kappa_3) &= K_{\nu-\lambda}(2\pi\kappa_2\kappa_3) - 2\pi\kappa_2\kappa_3 K_{\nu-\lambda+1}(2\pi\kappa_2\kappa_3), \\ \mathcal{D}_{\nu-\lambda}^{(4)}(2\pi\kappa_2\kappa_3) &= 3K_{\nu-\lambda}(2\pi\kappa_2\kappa_3) - 6(2\pi\kappa_2\kappa_3)K_{\nu-\lambda+1}(2\pi\kappa_2\kappa_3) \\ &\quad + (2\pi\kappa_2\kappa_3)^2 K_{\nu-\lambda+2}(2\pi\kappa_2\kappa_3), \\ \mathcal{D}_{\nu-\lambda}^{(6)}(2\pi\kappa_2\kappa_3) &= 15K_{\nu-\lambda}(2\pi\kappa_2\kappa_3) - 45(2\pi\kappa_2\kappa_3)K_{\nu-\lambda+1}(2\pi\kappa_2\kappa_3) \\ &\quad + 15(2\pi\kappa_2\kappa_3)^2 K_{\nu-\lambda+2}(2\pi\kappa_2\kappa_3) - (2\pi\kappa_2\kappa_3)^3 K_{\nu-\lambda+3}(2\pi\kappa_2\kappa_3). \end{aligned}$$

Numerical values of series (62) for parameters relevant to this paper:

$$\sum_{\mu \in \mathbf{Z}^2 \setminus \{0\}} |\mu|^{-3} = 9.03362168310095, \quad \sum_{\mu \in \mathbf{Z}^2 \setminus \{0\}} \mu_j^2 |\mu|^{-7} = 2.54512911683274$$

$$\begin{aligned}
\sum_{\mu \in \mathbf{Z}^2 \setminus \{0\}} |\mu|^{-5} &= 5.09025823366548, & \sum_{\mu \in \mathbf{Z}^2 \setminus \{0\}} \mu_j^2 |\mu|^{-9} &= 2.21155889383922 \\
\sum_{\mu \in \mathbf{Z}^2 \setminus \{0\}} |\mu|^{-7} &= 4.42311778767830, & \sum_{\mu \in \mathbf{Z}^2 \setminus \{0\}} \mu_j^2 |\mu|^{-11} &= 2.09563418137816 \\
\sum_{\mu \in \mathbf{Z}^2 \setminus \{0\}} |\mu|^{-9} &= 4.19126836275633, & \sum_{\mu \in \mathbf{Z}^2 \setminus \{0\}} \mu_j^4 |\mu|^{-11} &= 2.11729427669446 \\
\sum_{\mu \in \mathbf{Z}^2 \setminus \{0\}} \mu_j^6 |\mu|^{-15} &= 2.02776956400404, & \sum_{\mu \in \mathbf{Z}^2 \setminus \{0\}} \mu_j^4 |\mu|^{-13} &= 2.05039110312875
\end{aligned}$$

References

- [1] M. Abramowitz and I.A. Stegun. *Handbook of Mathematical Functions*. Dover Publications, Inc., New York, 1964. republication.
- [2] P. Cambray, K. Joulain, and G. Joulin. Mean evolution of wrinkle wavelengths in a model of weakly-turbulent premixed flame. *Combustion Science and Technology*, 103:265–282, 1994.
- [3] P. Cambray and G. Joulin. On moderately-forced premixed flames. In *Twenty-Fourth Symposium (International) on Combustion*, pages 61–67. The Combustion Institute, 1992.
- [4] P. Cambray and G. Joulin. Length-scales of wrinkling of weakly-forced, unstable premixed flames. *Combustion Science and Technology*, 97:405–428, 1994.
- [5] S. Gutman and G.I. Sivashinsky. The cellular nature of hydrodynamic flame instability. *Physica D*, 43:129–139, November 1990.
- [6] G. Joulin. On the hydrodynamic stability of curved premixed flames. *J. Phys. France*, 50:1069–1082, Mai 1989.
- [7] V. Karlin and G. Makhviladze. Computational analysis of the steady states of sivashinsky model of hydrodynamic flame instability. *Combustion Theory and Modelling*, 2001. (submitted).
- [8] V. Karlin and V. Maz’ya. Time-marching algorithms for nonlocal evolution equations based upon “approximate approximations”. *SIAM Journal on Scientific Computing*, 18(3):736–752, 1997.
- [9] V. Karlin, V. Maz’ya, A.B. Movchan, J.R. Willis, and R. Bullough. Numerical solution of nonlinear hypersingular integral equations of the Peierls type in dislocation theory. *SIAM Journal on Applied Mathematics*, 60(2):664–678, 2000.
- [10] L. Landau. On the theory of slow combustion. *Acta Physicochimica U.R.S.S.*, XIX(1):77–85, 1944.
- [11] G.H. Markstein. Experimental and theoretical studies of flame-front stability. *Journal of the Aeronautical Sciences*, 18:199–209, March 1951.

- [12] V. Maz'ya. Approximate approximations. In *Proceedings of the Eighth Conference on the Mathematics of Finite Elements and Applications VIII, MAFELAP 1993*, pages 77–104. Brunel University, 1994.
- [13] V. Maz'ya and G. Schmidt. On approximate approximations using Gaussian kernels. *IMA Journal on Numerical Analysis*, 16:13–29, 1996.
- [14] V. Maz'ya and G. Schmidt. Construction of basis functions for high order approximate approximations. In W. L. Wendland M. Bonnet, A.-M. Sändig, editor, *Mathematical Aspects of Boundary Element Methods*, CRC Research Notes in Mathematics, pages 191–202, London, 1999. Chapman & Hall.
- [15] D.M. Michelson and G.I. Sivashinsky. Thermal-expansion induced cellular flames. *Combustion and Flame*, 48:211–217, November 1982.
- [16] NAG Fortran Library. <http://www.nag.co.uk>.
- [17] NETLIB Public Software Library. <http://www.netlib.org>.
- [18] Z. Olami, B. Galanti, O. Kupervasser, and I. Procaccia. Random noise and pole dynamics in unstable front dynamics. *Physical Review E*, 55(3):2649–2663, March 1997.
- [19] A.P. Prudnikov, Yu.A. Brichkov, and O.I. Marichev. *Integrals and Series*, volume 1. Nauka, Moscow, 1981.
- [20] A.P. Prudnikov, Yu.A. Brichkov, and O.I. Marichev. *Integrals and Series*, volume 2. Gordon and Breach Science Publishers, New York, 1986.
- [21] M. Rahibe, N. Aubry, and G.I. Sivashinsky. Stability of pole solutions for planar propagating flames. *Physical Review E*, 54(5):4958–4972, November 1996.
- [22] M. Rahibe, N. Aubry, and G.I. Sivashinsky. Instability of pole solutions for planar propagating flames in sufficiently large domains. *Combustion Theory and Modelling*, 2(1):19–41, March 1998.
- [23] G.I. Sivashinsky. Nonlinear analysis of hydrodynamic instability in laminar flames - I. Derivation of basic equations. *Acta Astronautica*, 4:1177–1206, 1977.
- [24] G.I. Sivashinsky. Instabilities, pattern formation, and turbulence in flames. *Annual Reviews of Fluid Mechanics*, 15:179–199, 1983.
- [25] O. Thual, U. Frisch, and M. Hénon. Application of pole decomposition to an equation governing the dynamics of wrinkled flame fronts. *Le Journal de Physique*, 46(9):1485–1494, Septembre 1985.
- [26] L.N. Trefethen. Pseudospectra of linear operators. *SIAM Journal on Applied Mathematics*, 39(3):383–406, 1997.
- [27] D. Vaynblat and M. Matalon. Stability of pole solutions for planar propagating flames: I. Exact eigenvalues and eigenfunctions. *SIAM Journal on Applied Mathematics*, 60(2):679–702, 2000.